Supporting Information to:

Synthesis and Characterisation of a Mesocyclic Tripodal Triamine Ligand

Andrew D. Ure, Isabel Abánades Lázaro, Michelle Cotter and Aidan R. McDonald

Table of Contents

X-Ray Crystal Structure Refinement Details

Crystal Structure of 19·3HBr

A specimen of $C_{16}H_{44}Br_7N_6$, approximate dimensions 0.100 mm x 0.100 mm x 0.150 mm, was used for the X-ray crystallographic analysis. The X-ray intensity data were measured. The X-ray intensity data were measured at 100(2)K using an Oxford Cryosystems Cobra low temperature device using a MiTeGen micromount.

A total of 1119 frames were collected. The total exposure time was 4.66 hours. The integration of the data using a trigonal unit cell yielded a total of 25098 reflections to a maximum θ angle of 27.50° (0.77 Å resolution), of which 3863 were independent (average redundancy 6.497, completeness = 100.0%, R_{int} = 2.81%, R_{sig} = 1.87%) and 3298 (85.37%) were greater than $2\sigma(F^2)$.The final cell constants of a = 19.6192(13) Å, b = 19.6192(13) Å, c = 22.6973(15) Å, volume = 7566.0(11) $Å^3$, are based upon the refinement of the XYZ-centroids of reflections above 20 σ(I).The calculated minimum and maximum transmission coefficients (based on crystal size) are 0.5744 and 0.7457.
The structure was solved and refined using the Bruker SHELXTL Software Package, using the space group R -3, with Z = 9 for the formula unit, $C_{16}H_{44}Br_7N_6$.The final anisotropic full-matrix least-squares refinement on F^2 with 135 variables converged at R1 = 3.24%, for the observed data and wR2 = 7.56% for all data. The goodness-of-fit was 1.045. The largest peak in the final difference electron density synthesis was 2.749 $e^-/Å^3$ and the largest hole was -2.861 $e^-/Å^3$ with an RMS deviation of 0.110 $e^-/Å^3$. On the basis of the final model, the calculated density was 1.738 g/cm^3 and F(000), 3843 e^-.

Refinement Notes: The formula reflects the charge balance requirement of one HBr per 2 ($C_8H_{22}N_3$) (Br_6) unit. This hydrogen was not located on the difference map.

The unit cell contains an unknown solvent molecule(s) which has been treated as a diffuse contribution to the overall scattering without specific atom positions by SQUEEZE/PLATON. This consists of 321 electrons in a solvent accessible volume of 1126.5$Å^3$.

Crystal Structure of 16b

A specimen of $C_{22}H_{29}Br_{0.68}Cl_{0.32}N_2O_4S_2$, approximate dimensions 0.100 mm x 0.150 mm x 0.220 mm, was used for the X-ray crystallographic analysis. Bruker APEX software was used to correct for Lorentz and polarization effects.
A total of 2368 frames were collected. The total exposure time was 6.58 hours. The frames were integrated with the Bruker SAINT software package using a wide-frame algorithm. The integration of the data using a monoclinic unit cell yielded a total of 31099 reflections to a maximum θ angle of 68.37° (0.83 Å resolution), of which 4316 were independent
(average redundancy 7.206, completeness = 99.9%, R_{int} = 4.10%, R_{sig} = 2.39%) and 4110 (95.23%) were greater than $2\sigma(F^2)$.The final cell constants of a = 10.9261(5) Å, b = 12.7024(5) Å, c = 17.0382(7) Å, β = 96.0531(13)°, volume = 2351.51(17) $Å^3$, are based upon the refinement of the XYZ-centroids of 9937 reflections above 20 σ(I) with 8.137° < 2θ < 136.5°.Data were corrected for absorption effects using the multi-scan method (SADABS). The ratio of minimum to maximum apparent transmission was 0.832. The calculated minimum and maximum transmission coefficients (based on crystal size) are 0.6414 and 0.7531.
The structure was solved and refined using the Bruker SHELXTL Software Package, using the space group $P2_1/c$, with Z = 4 for the formula unit, $C_{22}H_{29}Br_{0.68}Cl_{0.32}N_2O_4S_2$.The final anisotropic

full-matrix least-squares refinement on F^2 with 303 variables converged at R1 = 4.88%, for the observed data and wR2 = 11.24% for all data. The goodness-of-fit was 1.098. The largest peak in the final difference electron density synthesis was 0.582 $e^-/Å^3$ and the largest hole was -0.386 $e^-/Å^3$ with an RMS deviation of 0.066 $e^-/Å^3$. On the basis of the final model, the calculated density was 1.455 g/cm^3 and F(000), 1073 e^-.

Refinement Note: Halide positions were modelled as half occupied with contraints (EADP) and restraints (DFIX) used to allow the model to converge. Each halide position was modelled as split between Br and Cl with refined occupancies of 0.35/0.15 Br1a/Cl1a and 0.33/0.17 Br1b/Cl1b.

Crystal Structure of [1b·H](PF_6)

A specimen of $C_{36}H_{44}F_6N_3P$, approximate dimensions 0.170 mm x 0.170 mm x 0.330 mm, was used for the X-ray crystallographic analysis. The X-ray intensity data were measured at 100(2)K using an Oxford Cryosystems Cobra low temperature device using a MiTeGen micromount. Bruker APEX software was used to correct for Lorentz and polarization effects.
A total of 4475 frames were collected. The total exposure time was 18.65 hours. The frames were integrated with the Bruker SAINT software package using a narrow-frame algorithm. The integration of the data using a monoclinic unit cell yielded a total of 122896 reflections to a maximum θ angle of 26.40° (0.80 Å resolution), of which 6919 were independent (average redundancy 17.762, completeness = 99.9%, R_{int} = 2.12%, R_{sig} = 0.72%) and 6244 (90.24%) were greater than $2\sigma(F^2)$.The final cell constants of a = 10.9164(3) Å, b = 16.2651(4) Å, c = 19.0039(5) Å, β = 93.2134(9)°, volume = 3368.96(15) Å^3, are based upon the refinement of the XYZ-centroids of 9805 reflections above 20 σ(I) with 4.893° < 2θ < 52.75°.Data were corrected for absorption effects using the multi-scan method (SADABS). The ratio of minimum to maximum apparent transmission was 0.964. The calculated minimum and maximum transmission coefficients (based on crystal size) are 0.7183 and 0.7454.
The structure was solved and refined using the Bruker SHELXTL Software Package, using the space group $P2_1/c$, with Z = 4 for the formula unit, $C_{36}H_{44}F_6N_3P$.The final anisotropic full-matrix least-squares refinement on F^2 with 451 variables converged at R1 = 4.82%, for the observed data and wR2 = 12.52% for all data. The goodness-of-fit was 1.059. The largest peak in the final difference electron density synthesis was 0.609 $e^-/Å^3$ and the largest hole was -0.425 $e^-/Å^3$ with an RMS deviation of 0.047 $e^-/Å^3$. On the basis of the final model, the calculated density was 1.309 g/cm^3 and F(000), 1400 e^-.

Refinement Note: PF_6 anion was disordered with the equatorial F atoms modelled in three positions with occupancies of 50:42:8%. The lowest occupancy moiety was held isotropic. Constraints were applied to occupancies (EADP) of the minor moieties.

Crystal Structure of [1b·2H]($OTf)_2$

A specimen of $C_{38}H_{45}F_6N_3O_6S_2$, approximate dimensions 0.220 mm x 0.240 mm x 0.260 mm, was used for the X-ray crystallographic analysis. The X-ray intensity data were measured at 100(2)K using an Oxford Cryosystems Cobra low temperature device using a MiTeGen micromount. Bruker APEX software was used to correct for Lorentz and polarization effects.
A total of 2292 frames were collected. The total exposure time was 12.73 hours. The integration of the data using a monoclinic unit cell yielded a total of 185743 reflections to a maximum θ angle of 30.60° (0.70 Å resolution), of which 11856 were independent (average redundancy 15.667, completeness = 99.8%, R_{int} = 3.81%, R_{sig} = 1.73%) and 9748 (82.22%) were greater than $2\sigma(F^2)$. The final cell constants of a = 11.1337(5) Å, b = 24.2066(10) Å, c =

15.0351(6) Å, β = 107.5700(10)°, volume = 3863.1(3) $Å^3$, are based upon the refinement of the XYZ-centroids of reflections above 20 σ(I). Data were corrected for absorption effects using the multi-scan method (SADABS). The calculated minimum and maximum transmission coefficients (based on crystal size) are 0.6953 and 0.7461.
The structure was solved and refined using the Bruker SHELXTL Software Package, using the space group $P2_1/c$, with Z = 4 for the formula unit, $C_{38}H_{45}F_6N_3O_6S_2$. The final anisotropic full-matrix least-squares refinement on F^2 with 505 variables converged at R1 = 3.72%, for the observed data and wR2 = 9.89% for all data. The goodness-of-fit was 1.039. The largest peak in the final difference electron density synthesis was 0.502 $e^-/Å^3$ and the largest hole was -0.377 $e^-/Å^3$ with an RMS deviation of 0.051 $e^-/Å^3$. On the basis of the final model, the calculated density was 1.406 g/cm^3 and F(000), 1712 e^-.

Refinement Note: Hydrogen atoms H8 and H11 were located and refined.

References:

Bruker APEX v2014.11-0, Bruker AXS Inc., Madison, Wisconsin, USA.
SADABS (2014/5) Bruker AXS Inc., Madison, Wisconsin, USA; Sheldrick, G. M. University of Göttingen, Germany.
SHELXL-2014, (2014), Bruker AXS Inc., Madison, Wisconsin, USA; Sheldrick, G. M. University of Göttingen, Germany.

Table S1 - Crystal data and refinement parameters for the reported crystal structures.

	19•3HBr	**16b**	[**1b**•H]PF_6	[**1b**•2H]OTf_2
Empirical formula	$C_{16}H_{45}Br_7N_6$	$C_{22}H_{29}Br_{0.68}Cl_{0.32}N_2O_4S_2$	$C_{36}H_{44}F_6N_3P$	$C_{38}H_{45}F_6N_3O_6S_2$
fw	879.94	515.05	663.71	817.89
Crystal System	Trigonal	Monoclinic	Monoclinic	Monoclinic
SG	R -3	$P2_1/c$	$P2_1/c$	$P2_1/c$
a (Å)	19.6192(13)	10.9261(5)	10.9164(3)	11.1337(5)
b (Å)	19.6192(13)	12.7024(5)	16.2651(4)	24.2066(10)
c (Å)	22.6973(15)	17.0382(7)	19.0039(5)	15.0351(6)
α (°)	90	90	90	90
β (°)	90	96.0531(13)	93.2134(9)	107.5700(10)
γ (°)	120	90	90	90
V ($Å^3$)	7566.0(11)	2351.51(17)	3368.96(15)	3863.1(3)
T (K)	100(2)	100(2)	100(2)	100(2)
Z	9	4	4	4
ρ (g/cm^3)	1.738	1.455	1.309	1.406
μ (mm^{-1})	8.366	3.996	0.145	0.217
Total reflns	25098	31099	122896	185743
Indep. reflns	3863	4316	6919	11856
R(int)	0.0281	0.0410	0.0212	0.0381
R_1[a] [I>2σ(I)]	0.0324	0.0488	0.0482	0.0372
wR_2 [I>2σ(I)]	0.0777	0.1115	0.1204	0.0899

[a]$R_1 = \Sigma||F_o| - |F_c||/\Sigma|F_o|$, $wR_2 = \Sigma\,[w(F_o^2 - F_c^2)^2/\Sigma w(F_o^2)^2]^{1/2}$.

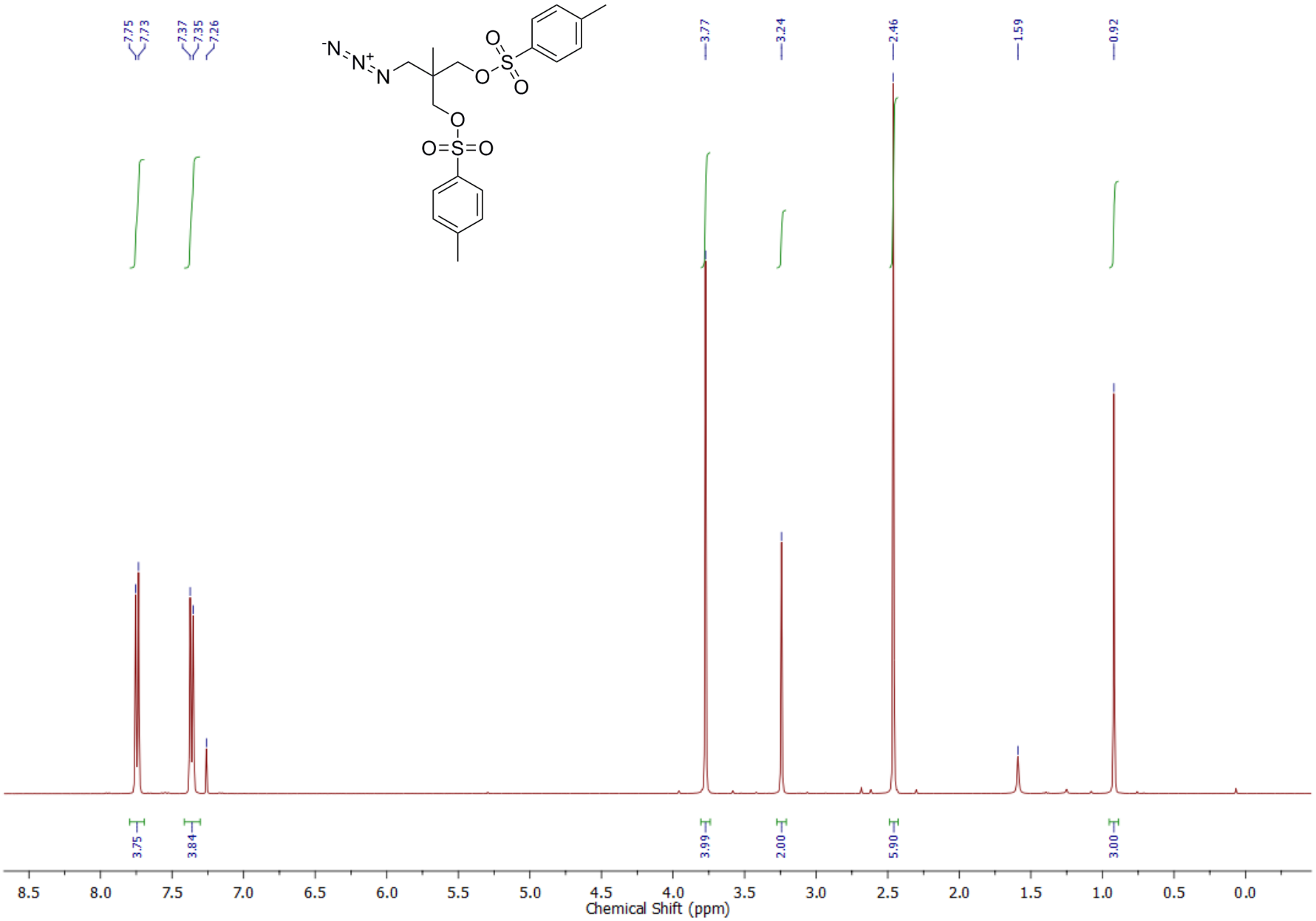

Figure S1—^{1}H NMR Spectrum of **7**, $CDCl_3$, 400 MHz

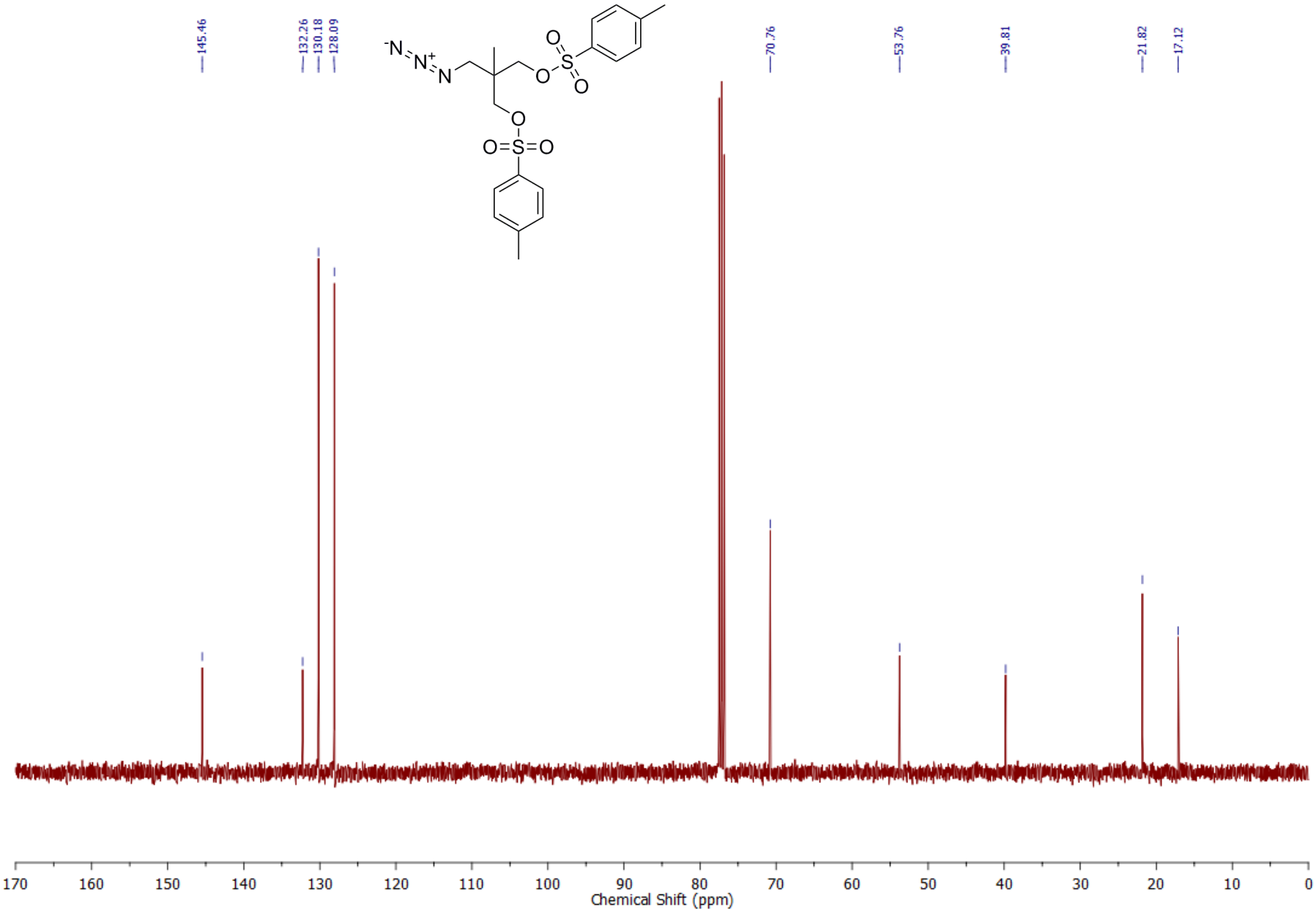

Figure S2—^{13}C NMR Spectrum of **7**, $CDCl_3$, 101 MHz

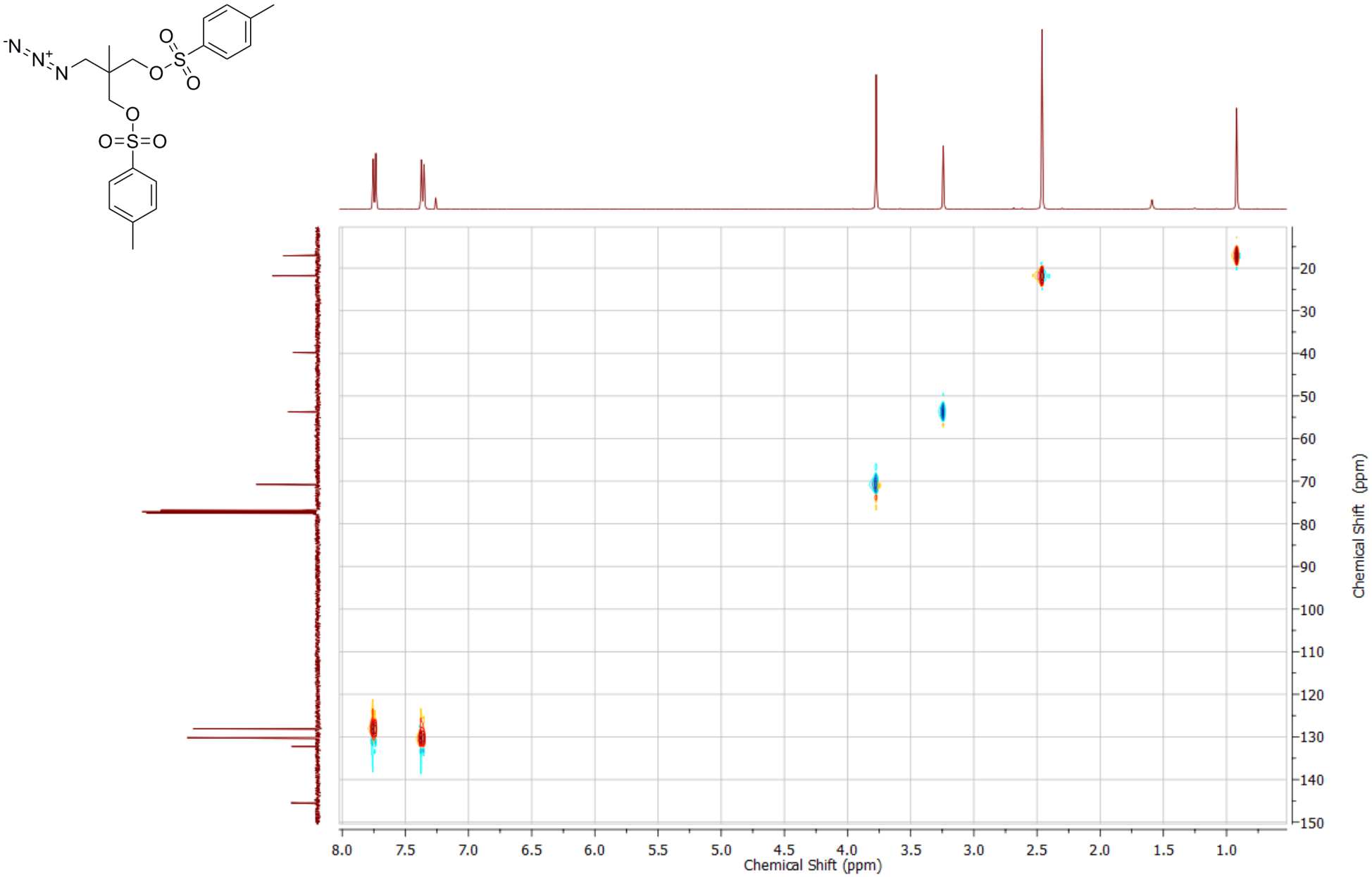

Figure S3—HSQC NMR Spectrum of **7**, $CDCl_3$, 400 MHz

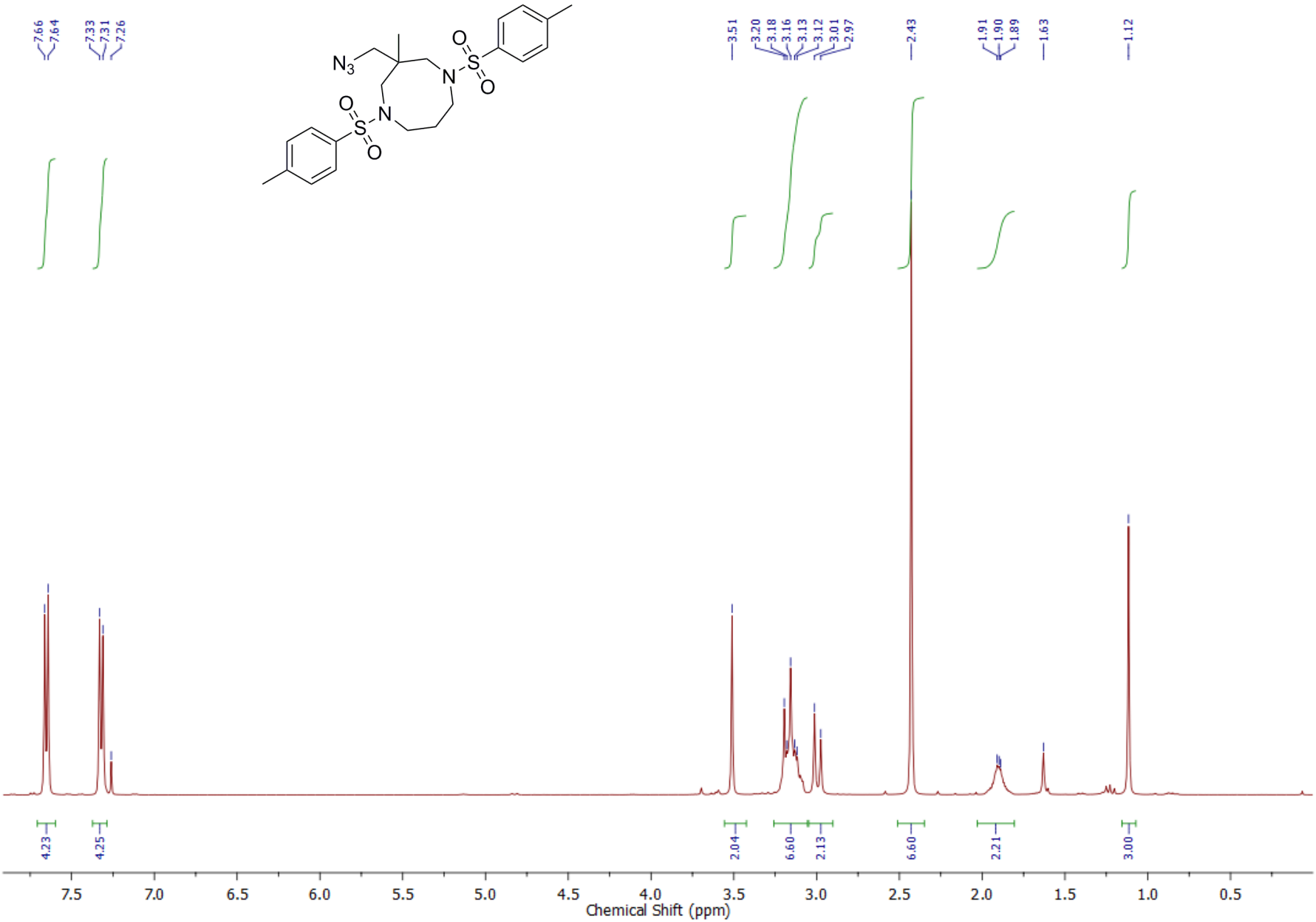

Figure S4—^{1}H NMR Spectrum of **8**, $CDCl_3$, 400 MHz

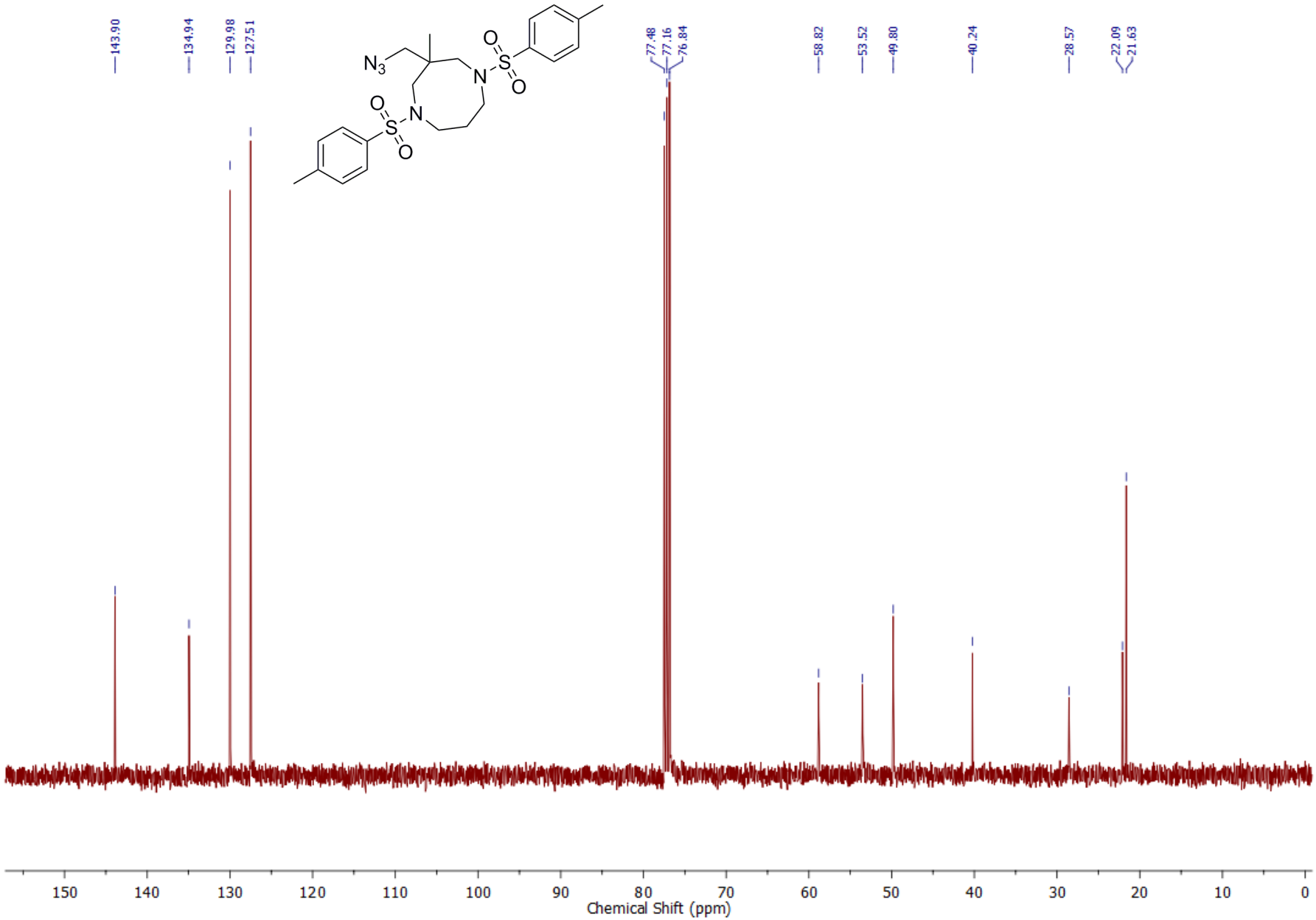

Figure S5—^{13}C NMR Spectrum of **8**, $CDCl_3$, 101 MHz

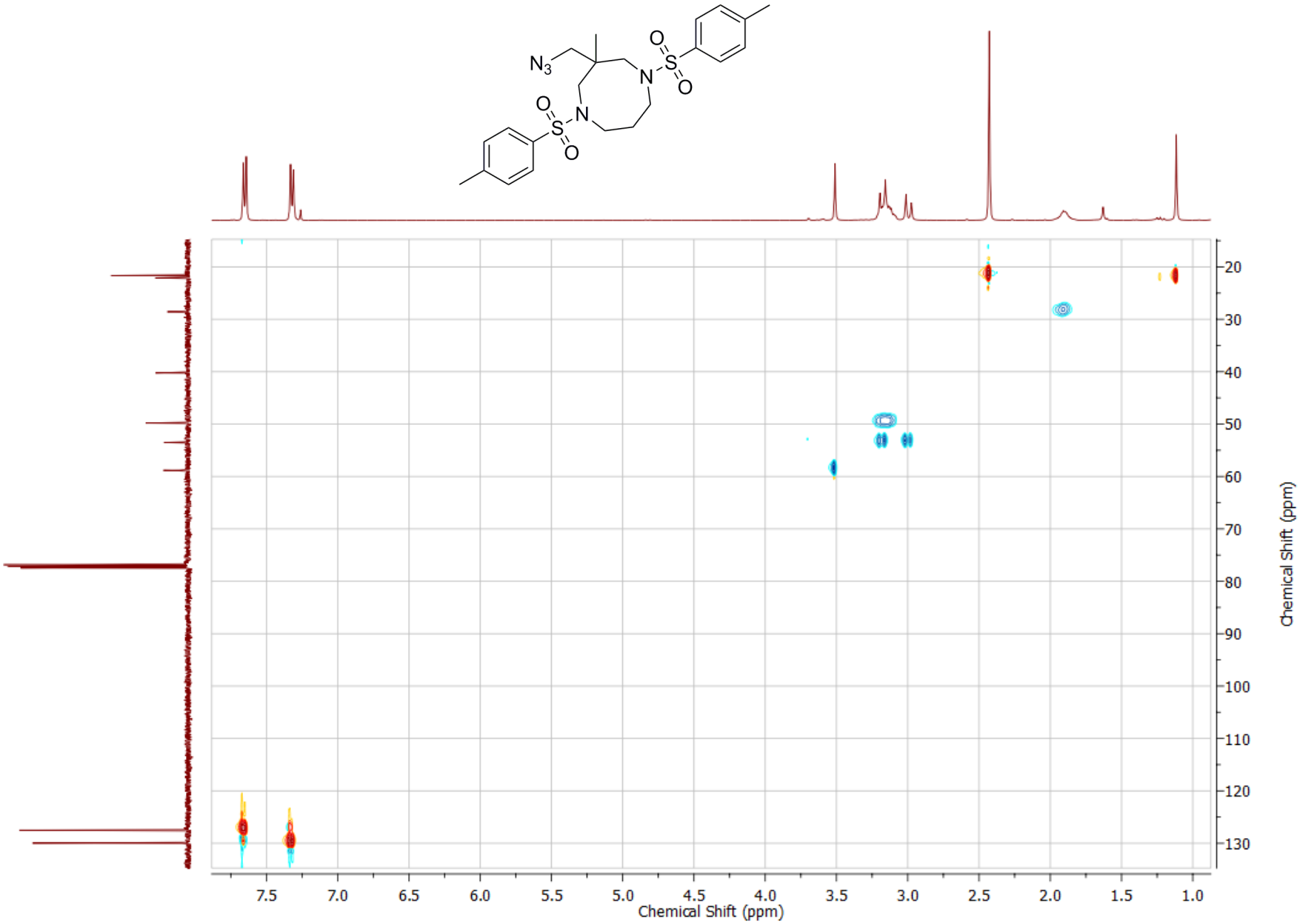

Figure S6—HSQC NMR Spectrum of **8**, $CDCl_3$, 400 MHz

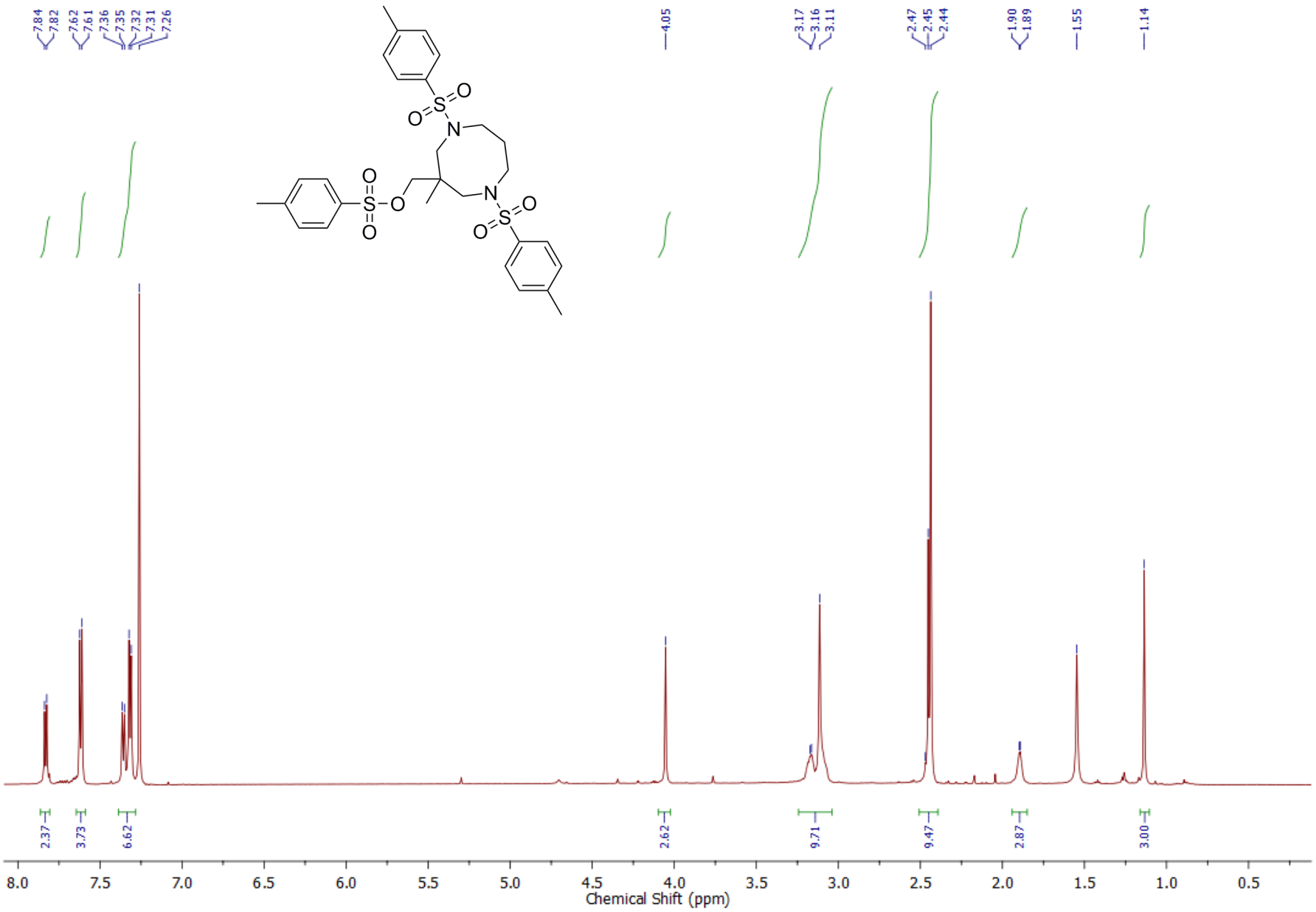

Figure S7—^{1}HNMR Spectrum of **16a**, $CDCl_3$, 600 MHz

Figure S8—^{13}CNMR Spectrum of **16a**, $CDCl_3$, 151 MHz

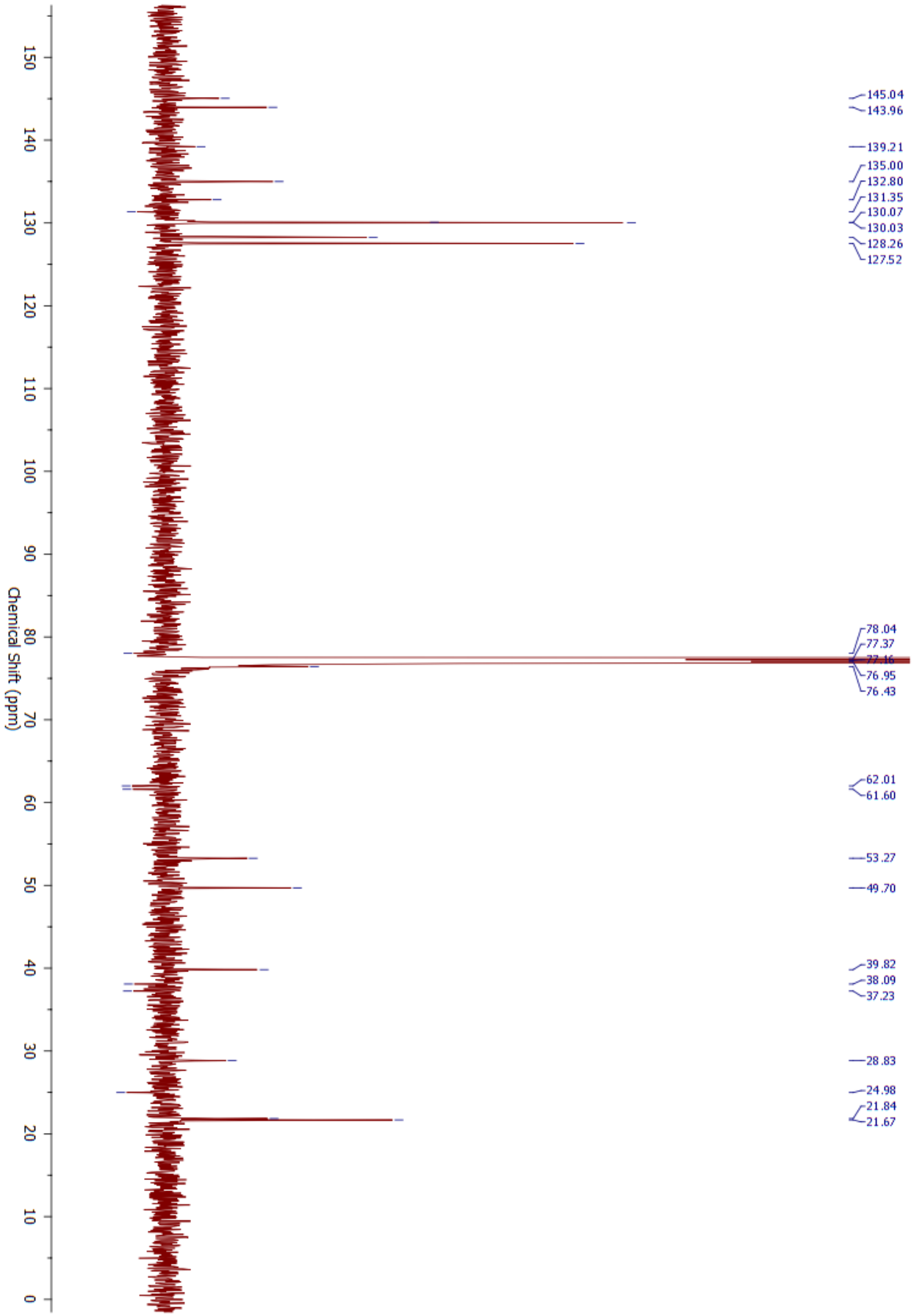

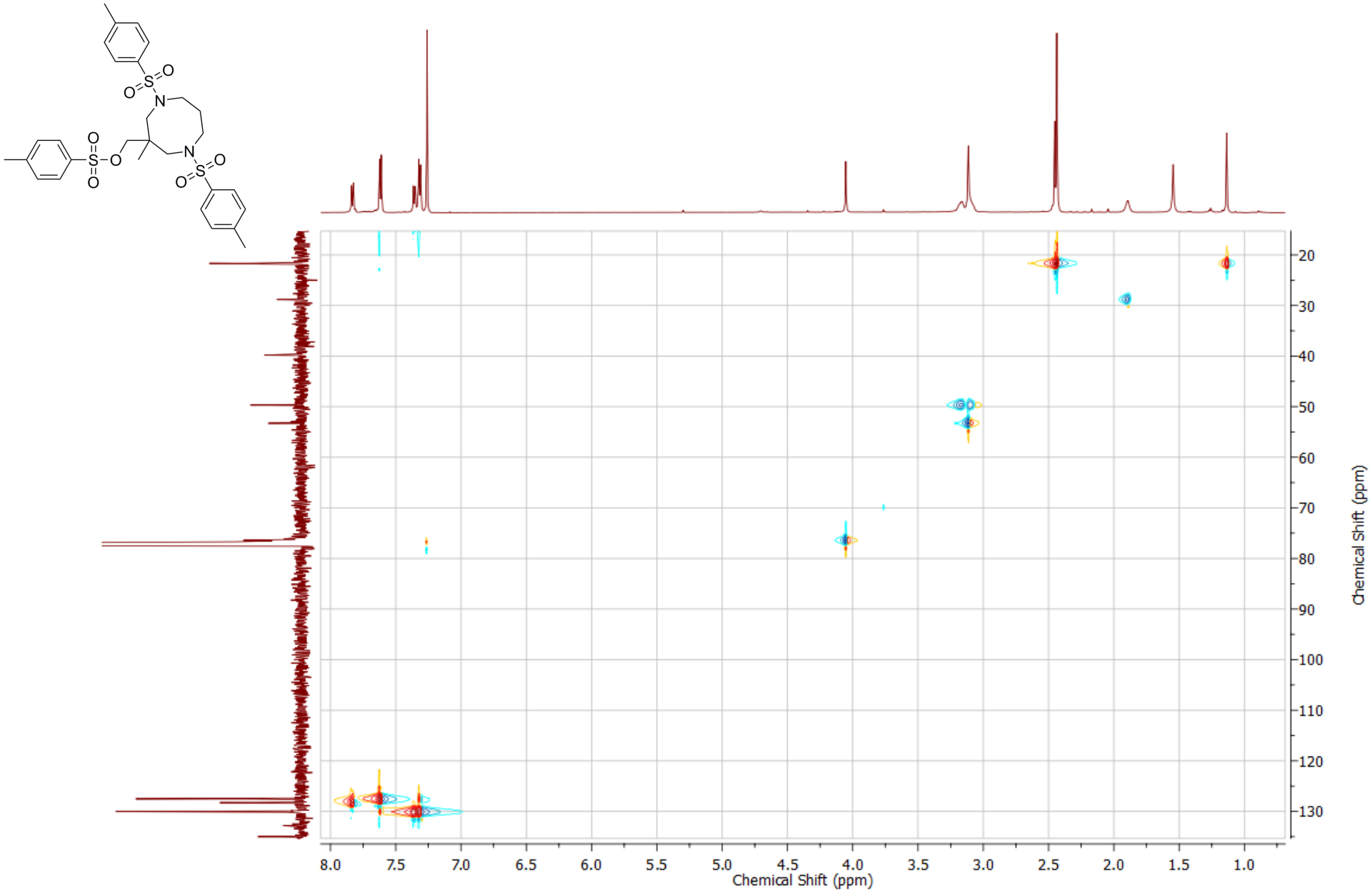

Figure S9—HSQC Spectrum of **16a**, $CDCl_3$, 600 MHz

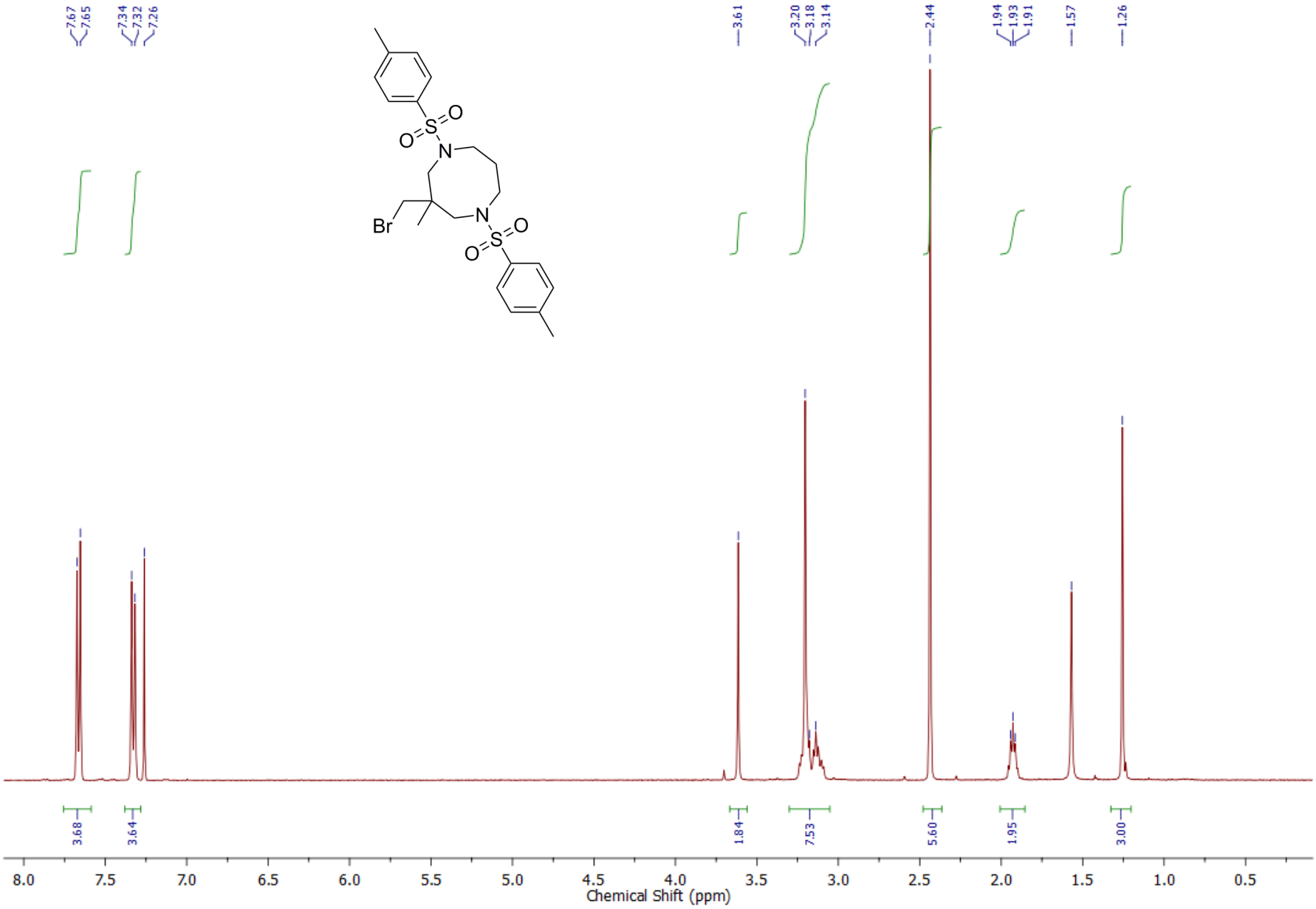

Figure S10—^{1}H NMR Spectrum of **16b**, $CDCl_3$, 400 MHz

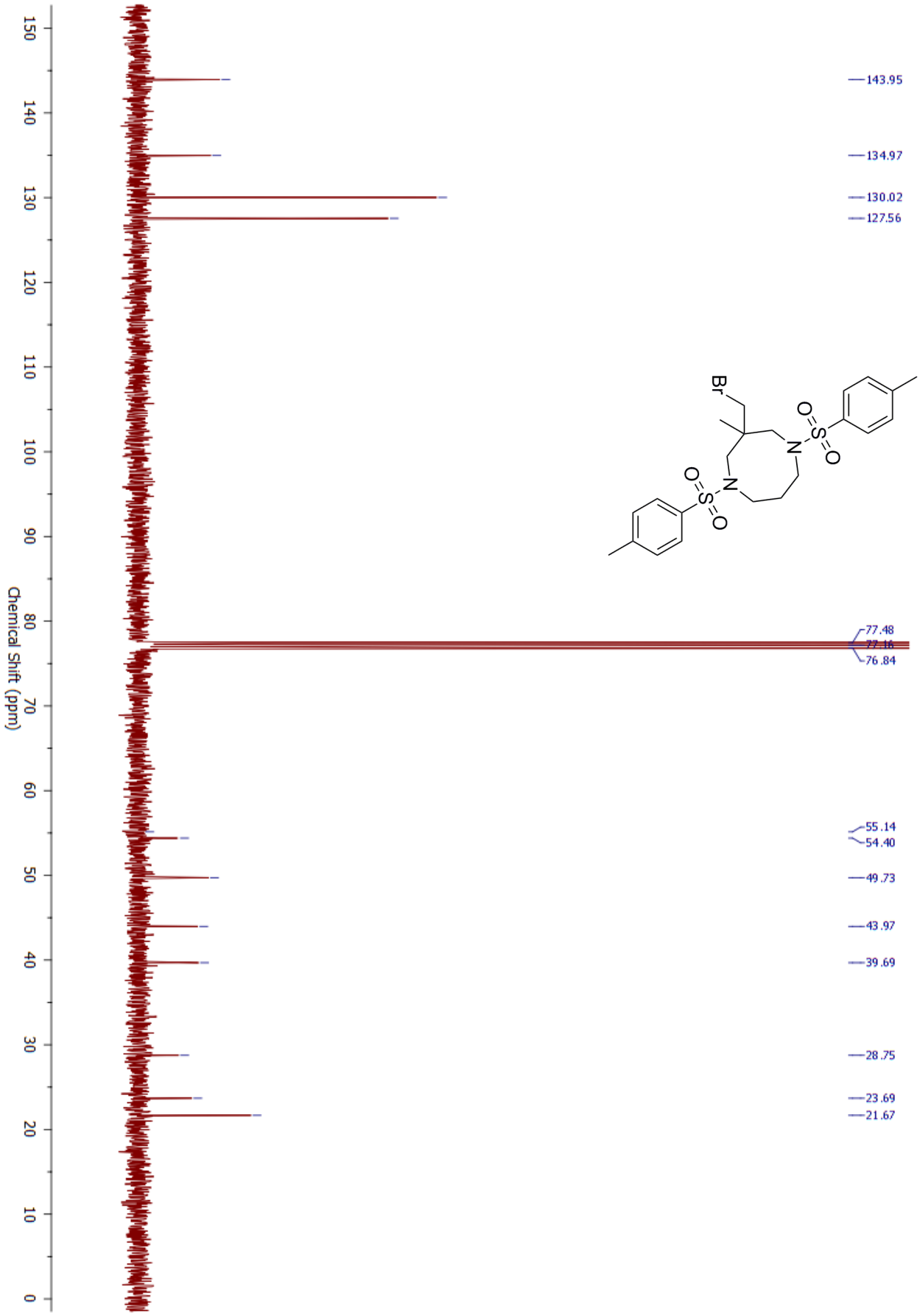

Figure S11—^{13}C NMR Spectrum of **16b**, $CDCl_3$, 101 MHz

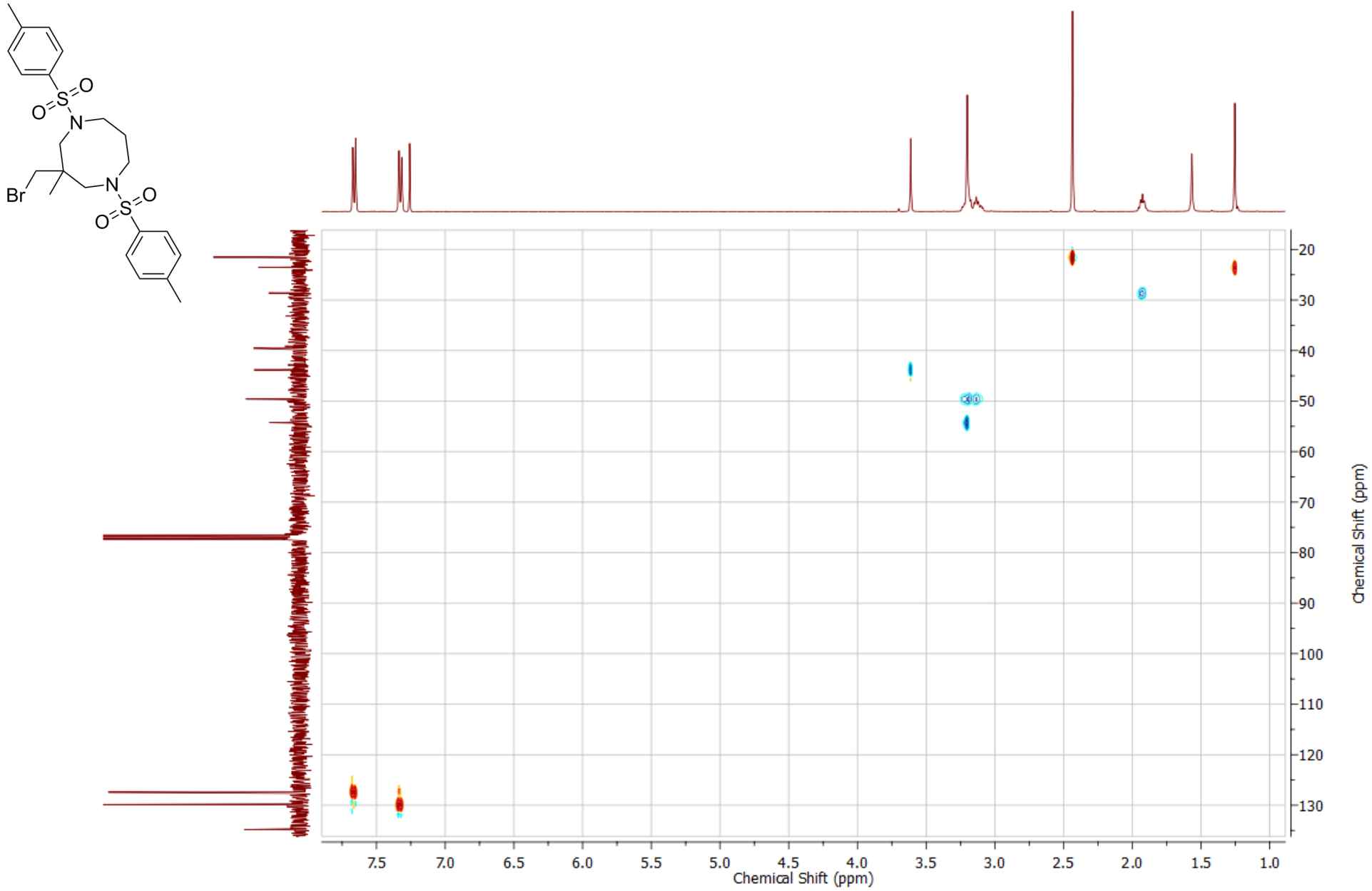

Figure S12—HSQC NMR Spectrum of **16b**, $CDCl_3$, 400 MHz

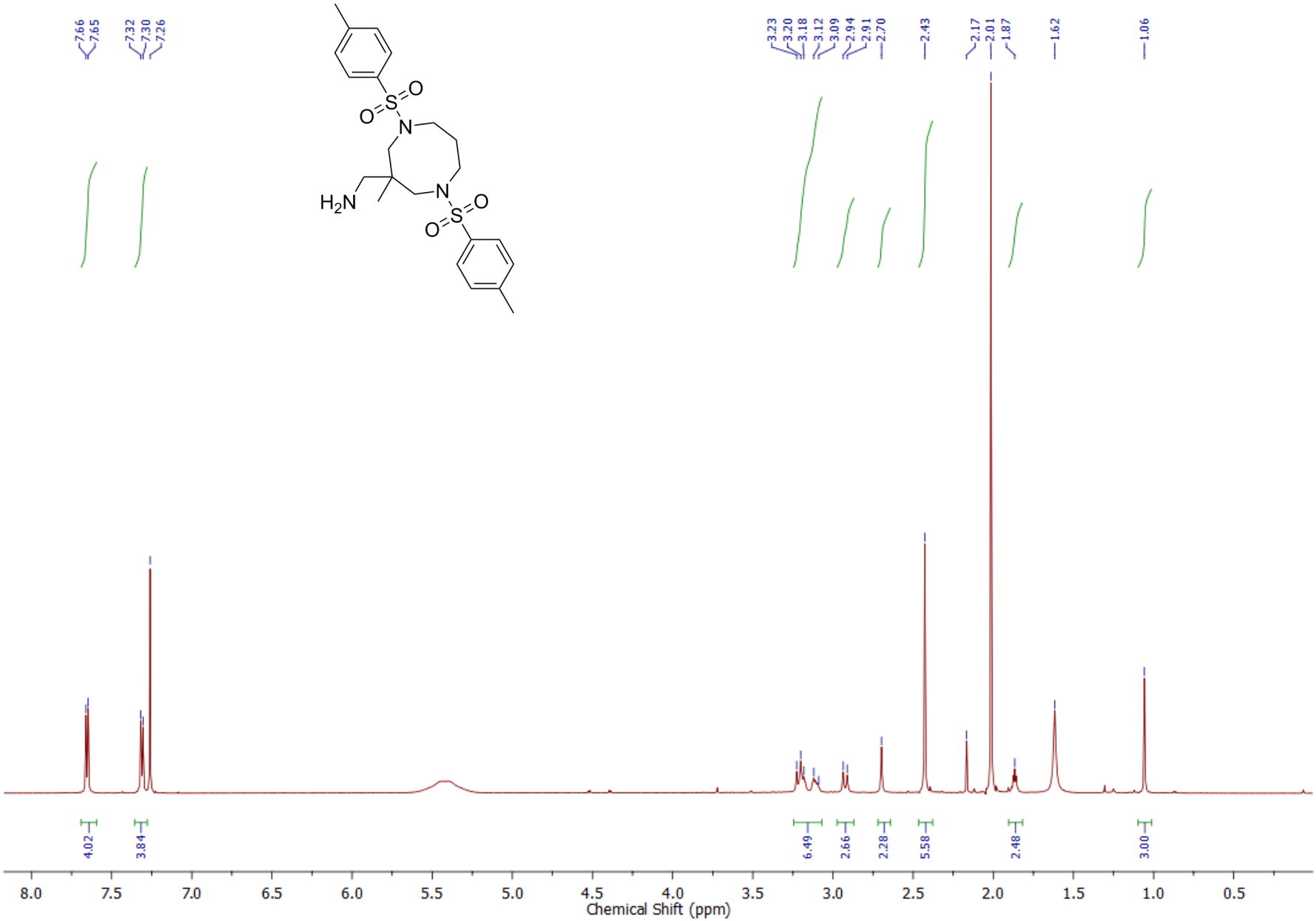

Figure
S13—^{1}H NMR Spectrum of **17**, $CDCl_3$, 400 MHz

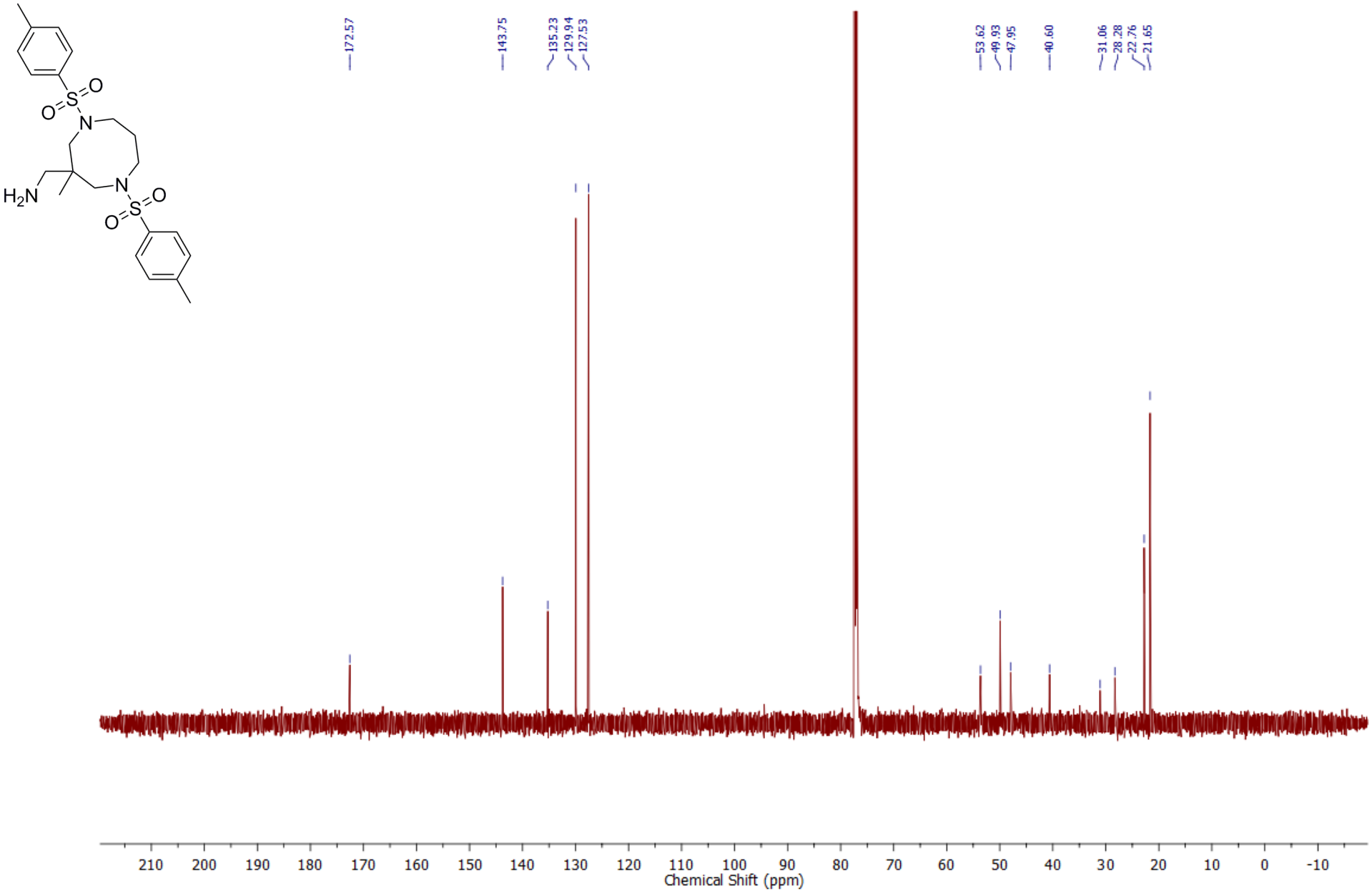

Figure
S14—^{13}C NMR Spectrum of **17**, $CDCl_3$, 101 MHz

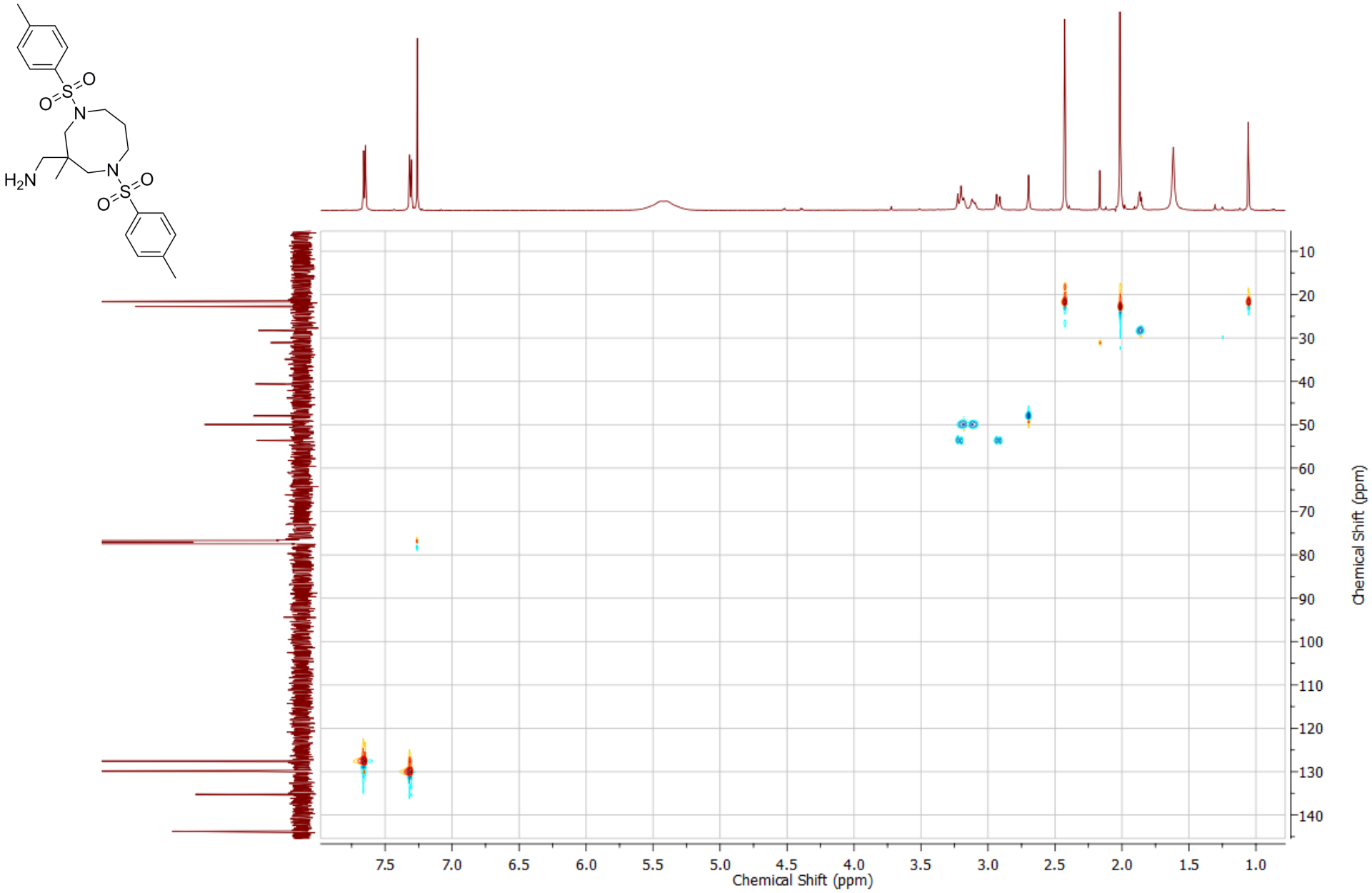

Figure S15—HSQC NMR Spectrum of **17**, $CDCl_3$, 400 MHz

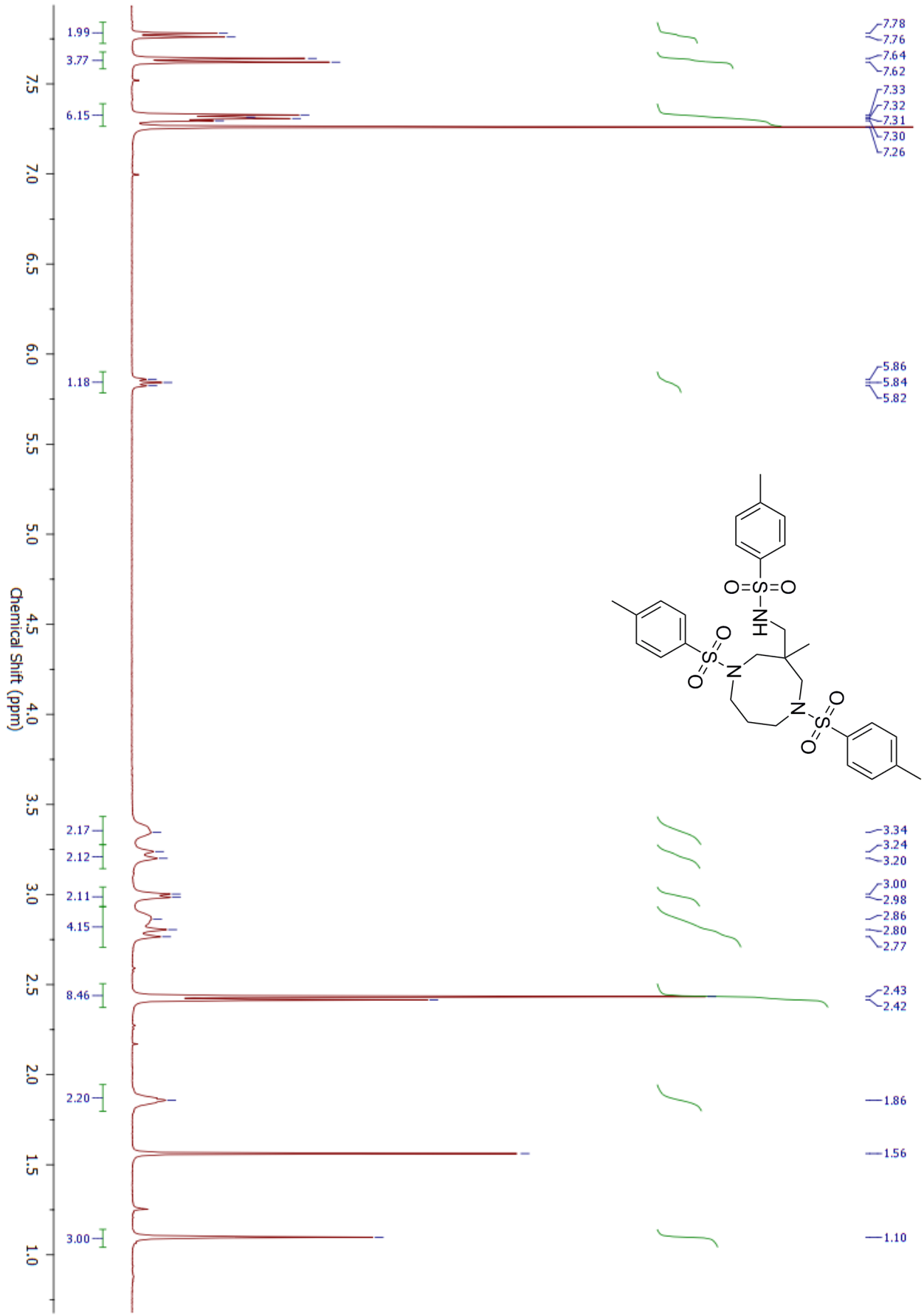

Figure S16—^{1}H NMR Spectrum of **18**, $CDCl_3$, 400 MHz

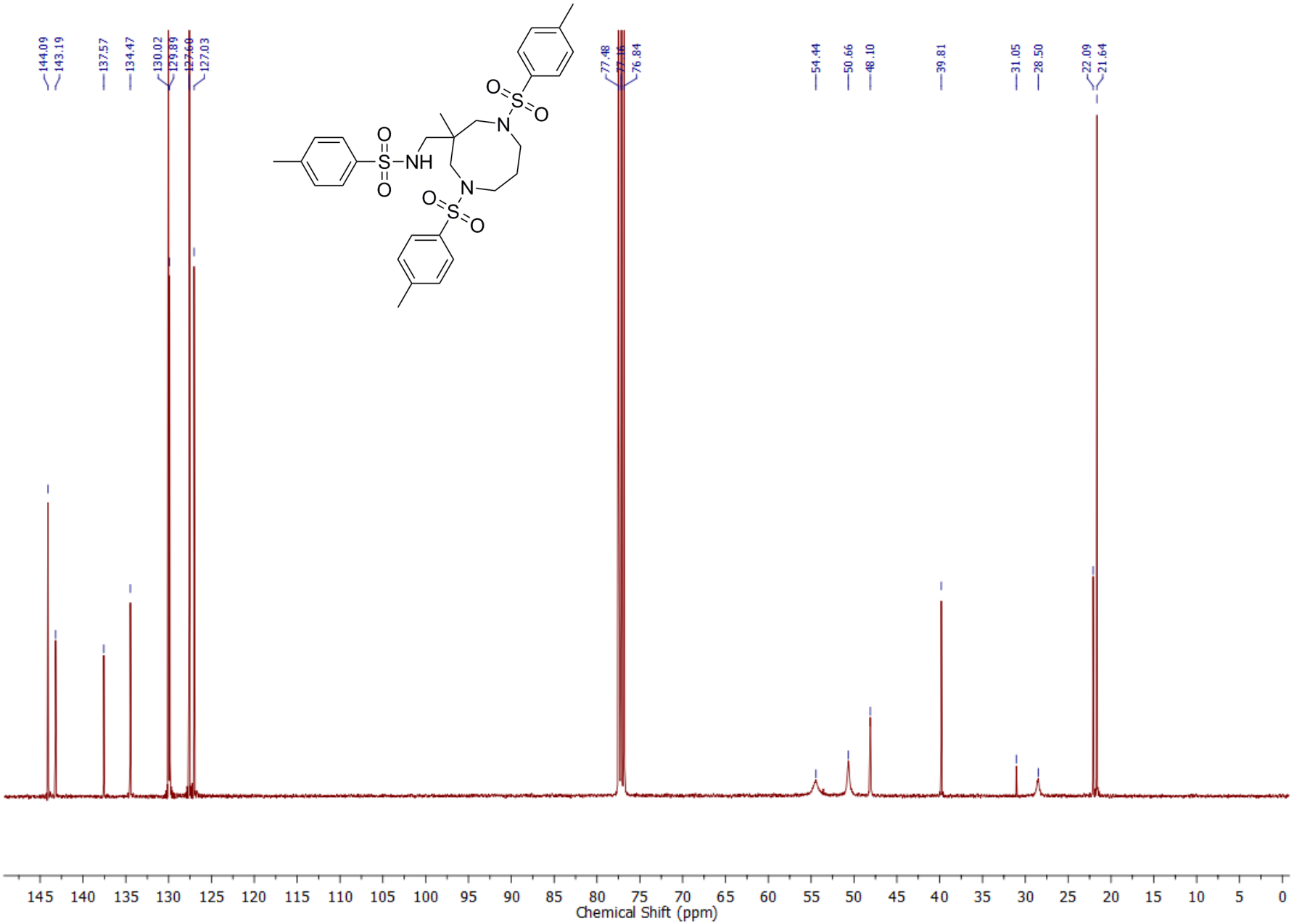

Figure S17—^{13}C NMR Spectrum of **18**, $CDCl_3$, 101 MHz

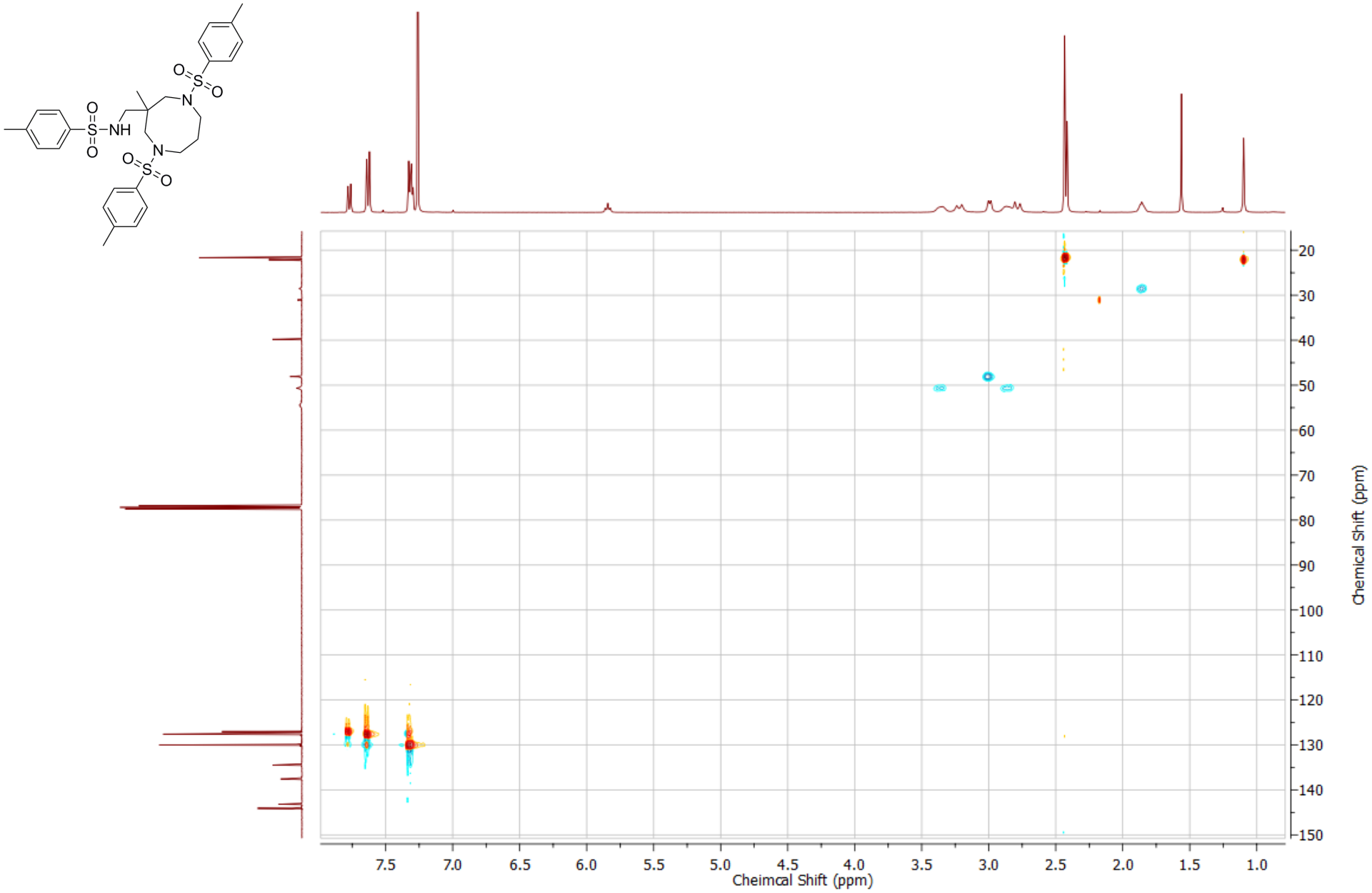

Figure S18—HSQC NMR Spectrum of **18**, $CDCl_3$, 400 MHz

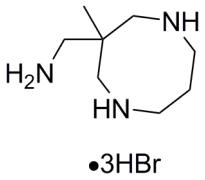

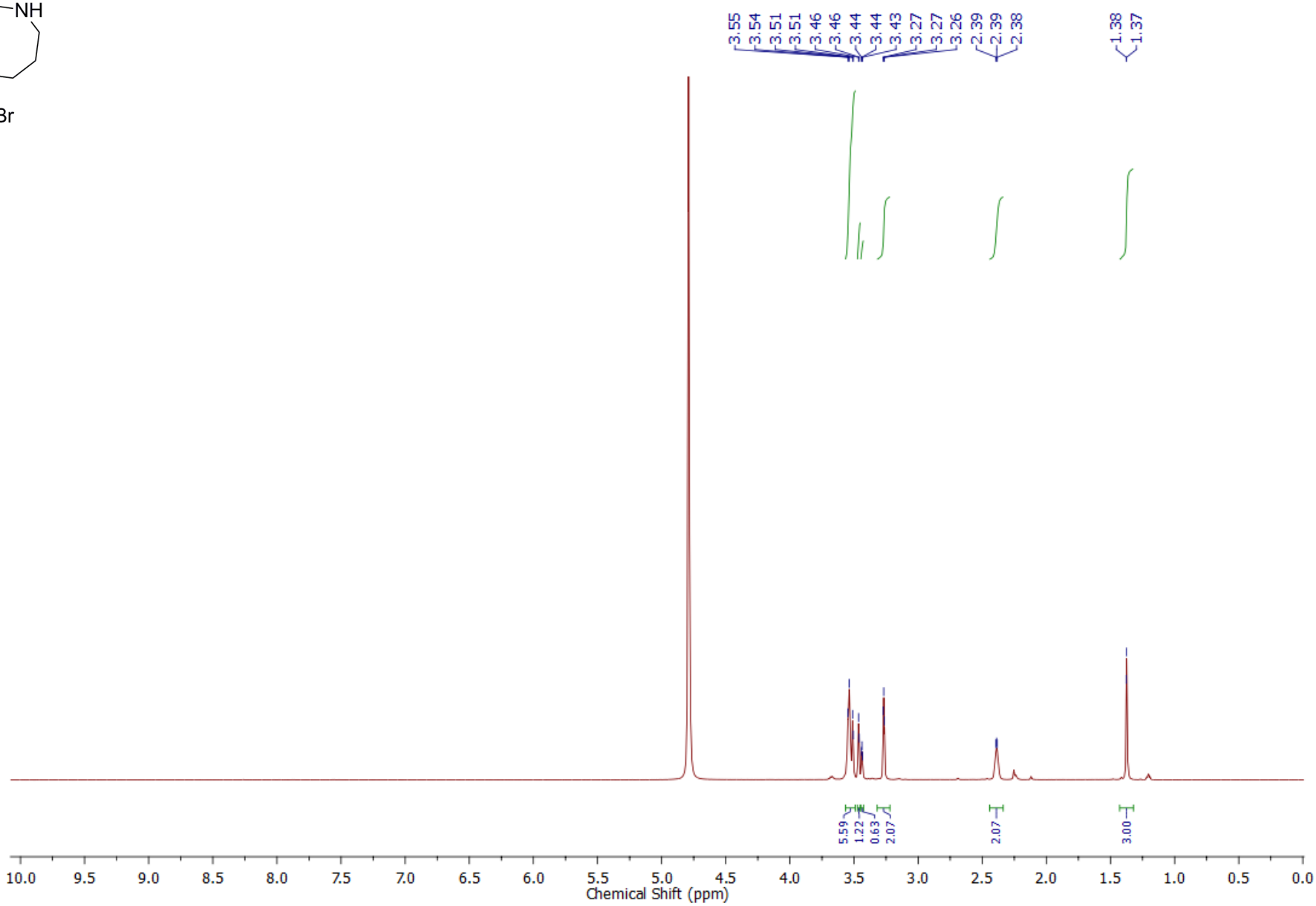

Figure S19—^{1}H NMR Spectrum of **19·3HBr**, D_2,O 600 MHz

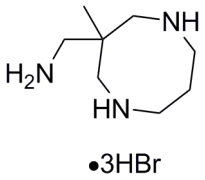

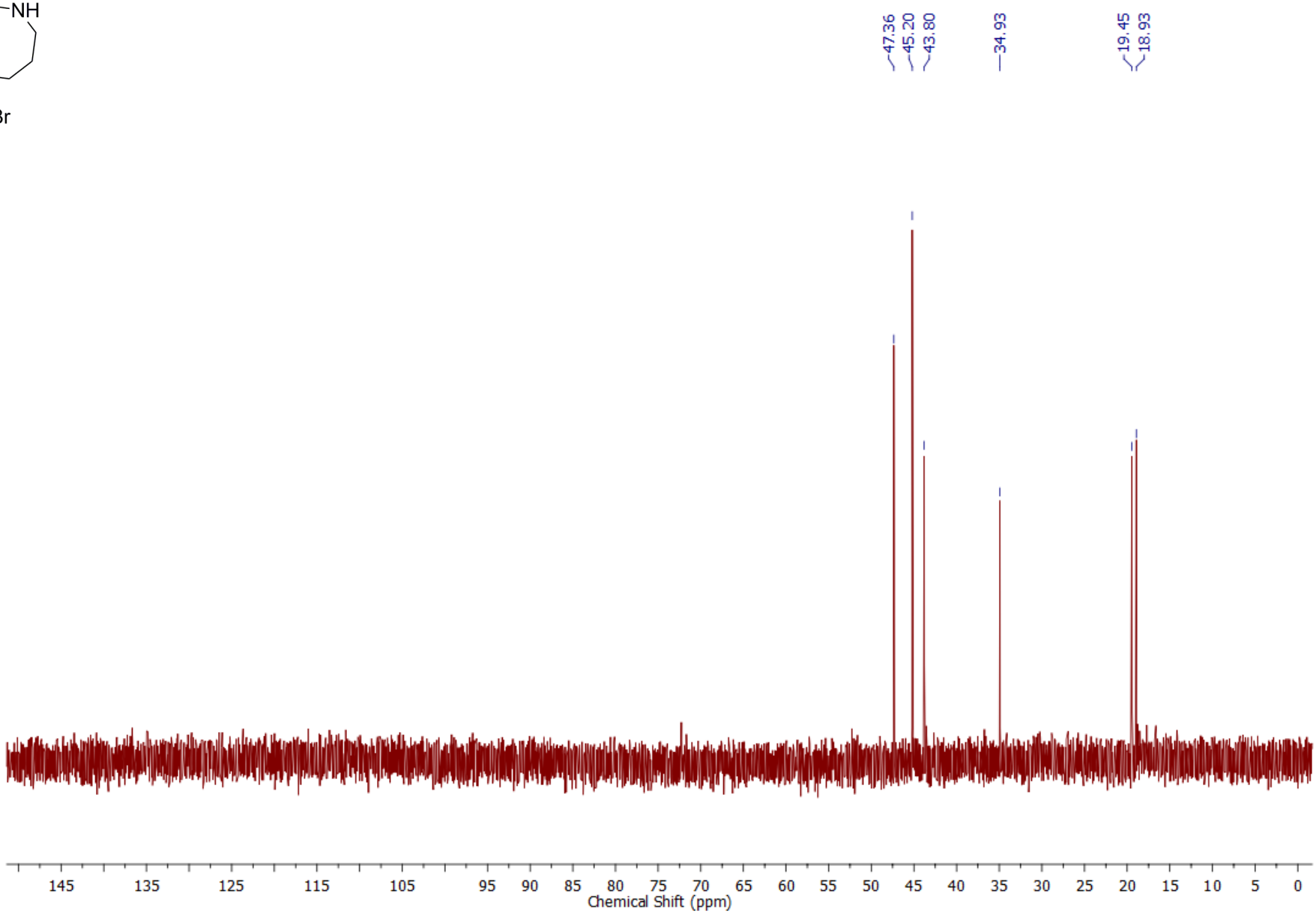

Figure S120—^{13}C NMR Spectrum of **19·3HBr**, D_2,O 151 MHz

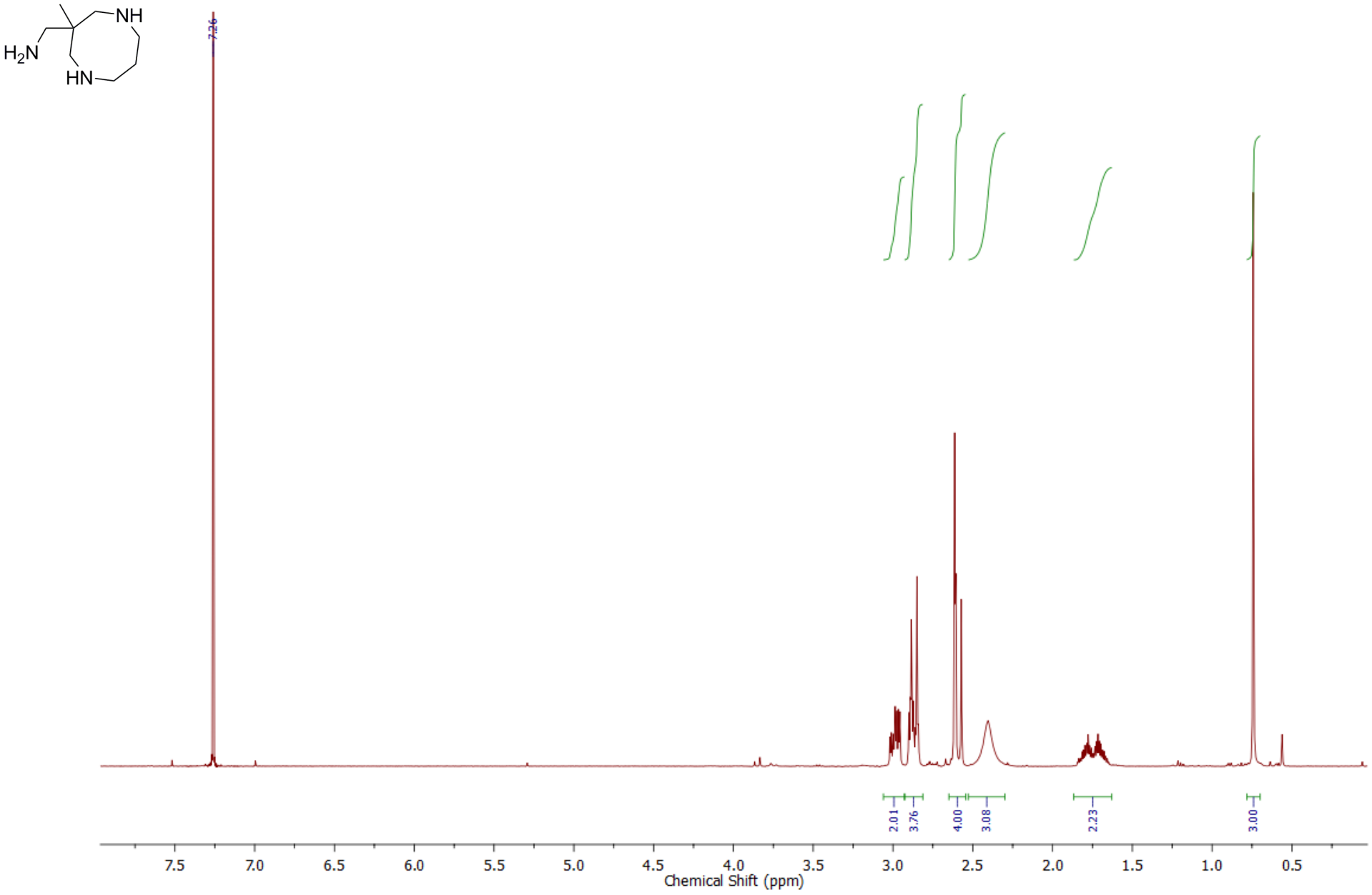

Figure S21—^{1}H NMR Spectrum of **19**, $CDCl_3$, 400 MHz

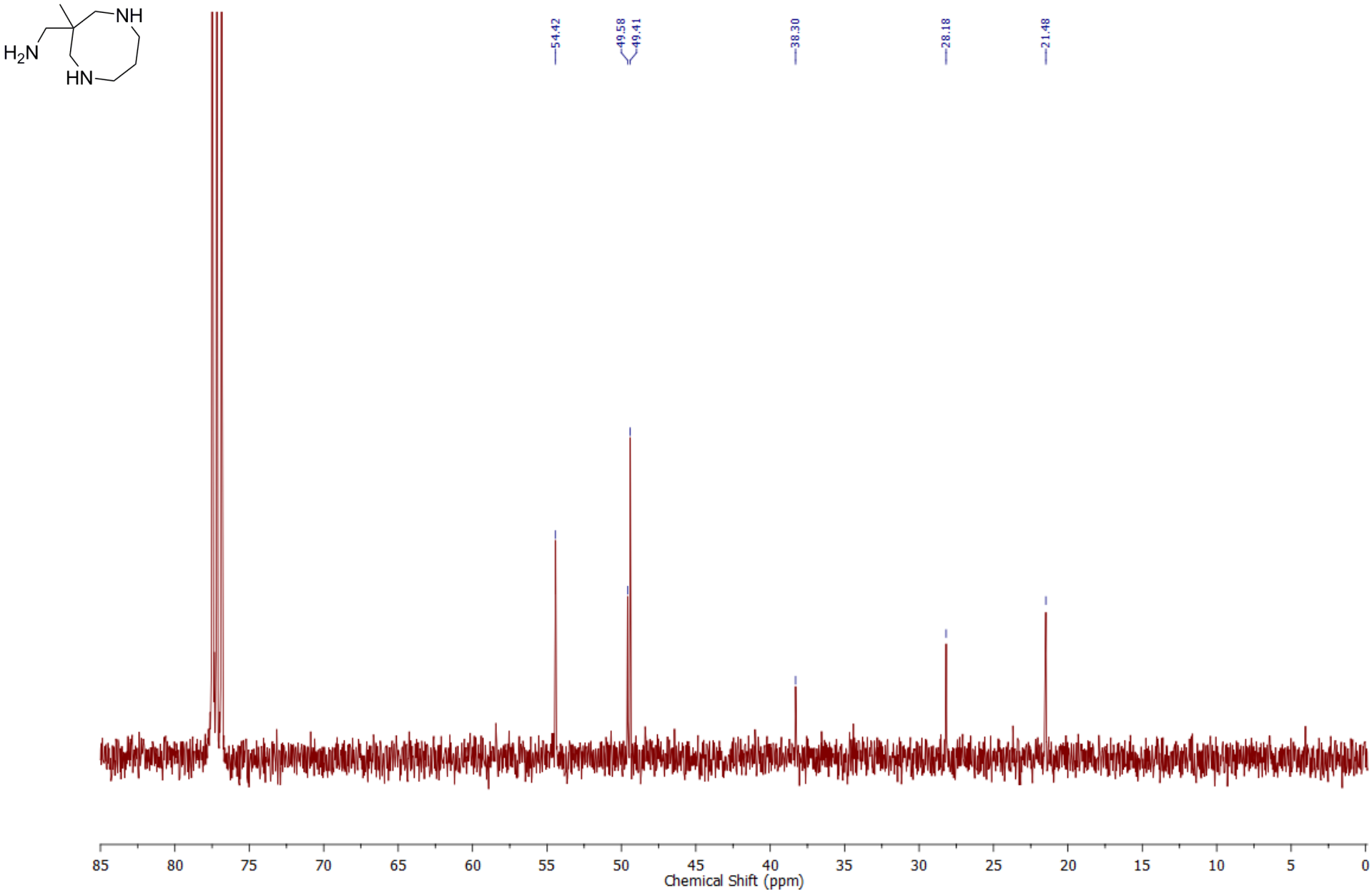

Figure S22—^{13}C NMR Spectrum of **19**, $CDCl_3$, 101 MHz

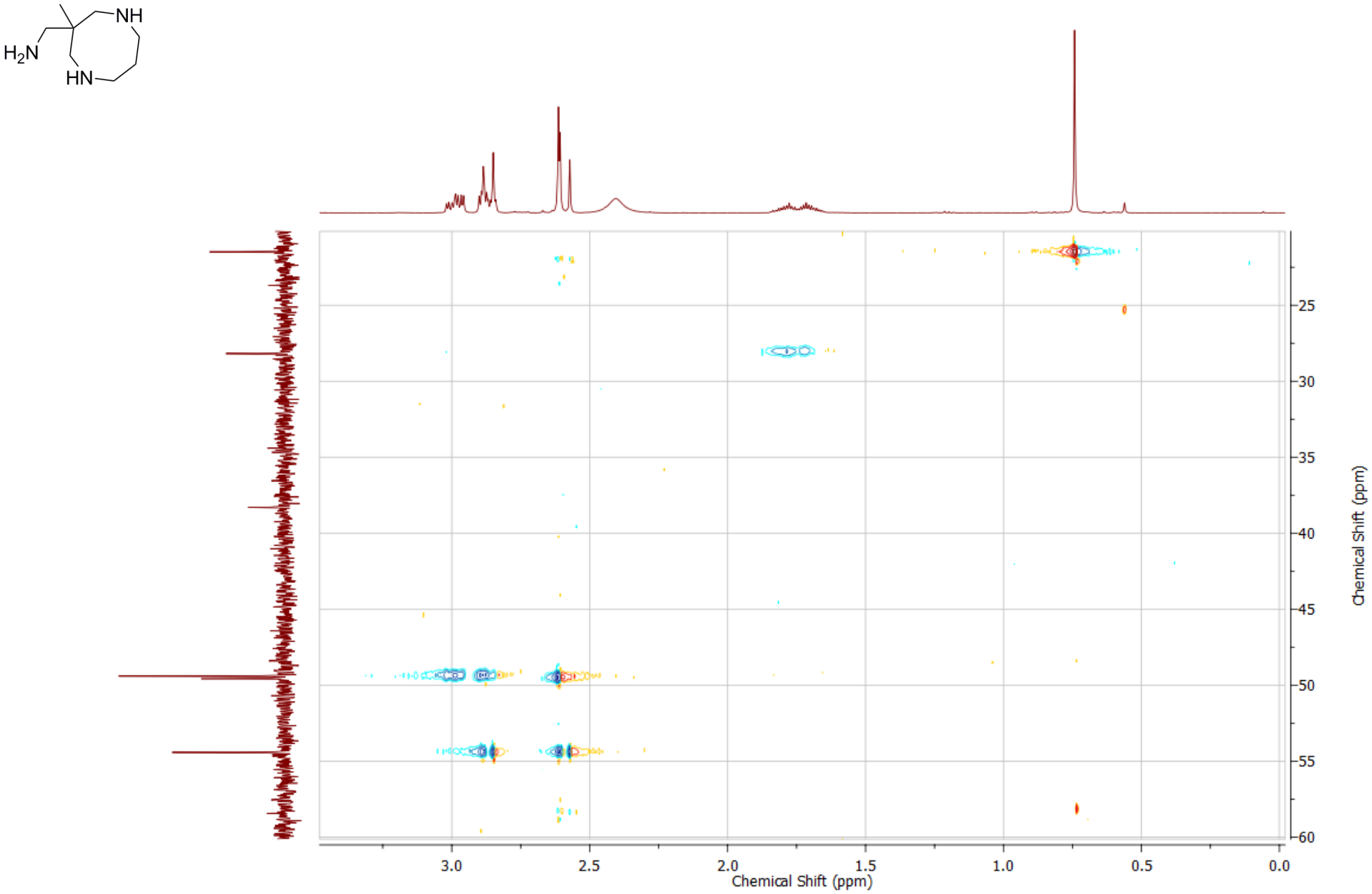

Figure S23—HSQC NMR Spectrum of **19**, $CDCl_3$, 400 MHz

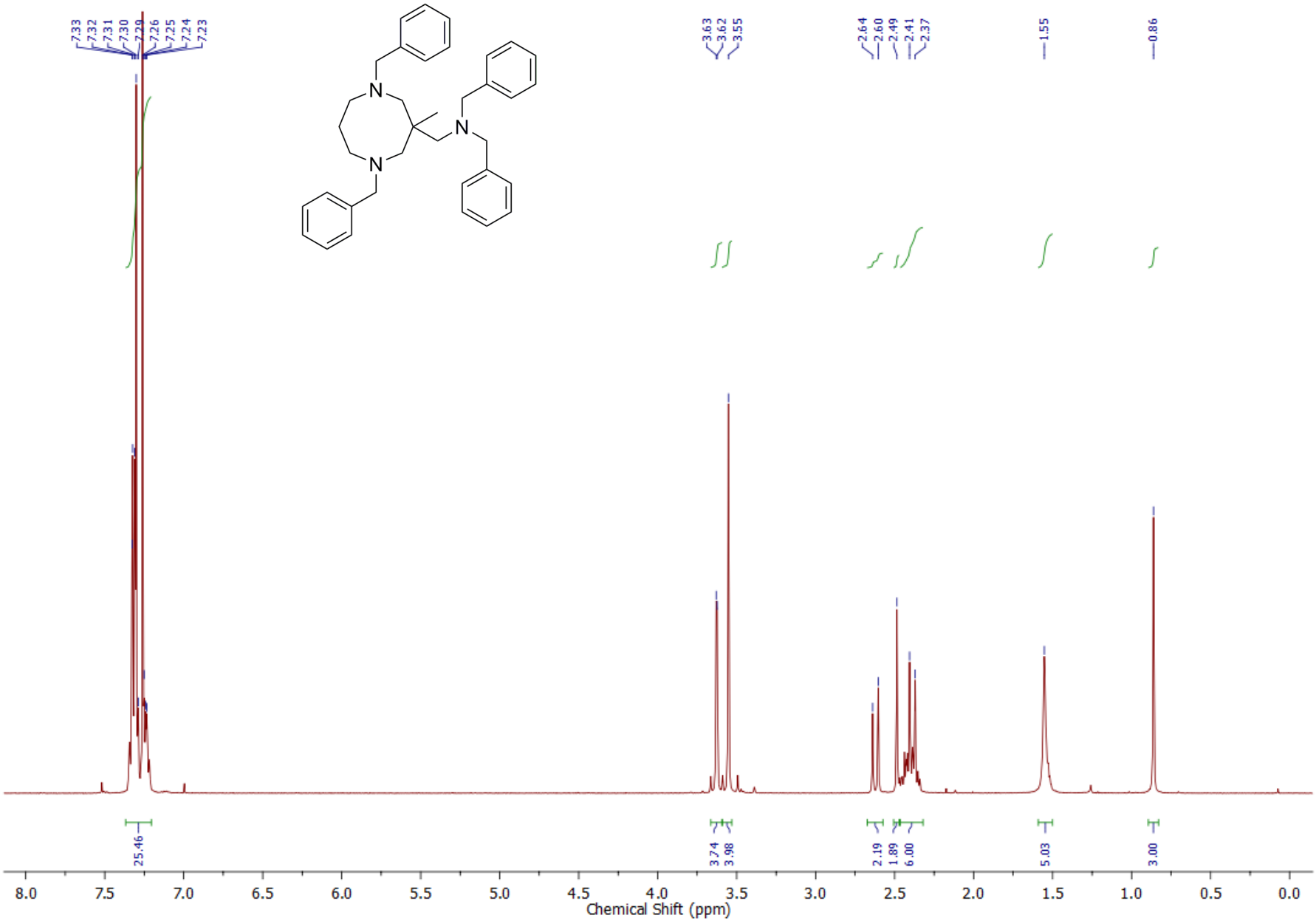

Figure S24—^{1}H NMR Spectrum of **1b**, $CDCl_3$, 400 MHz. The H_2O peak covers the signal from $H_{4/4'}$ however, this signal can clearly be identified from the HSQC (Figure S26).

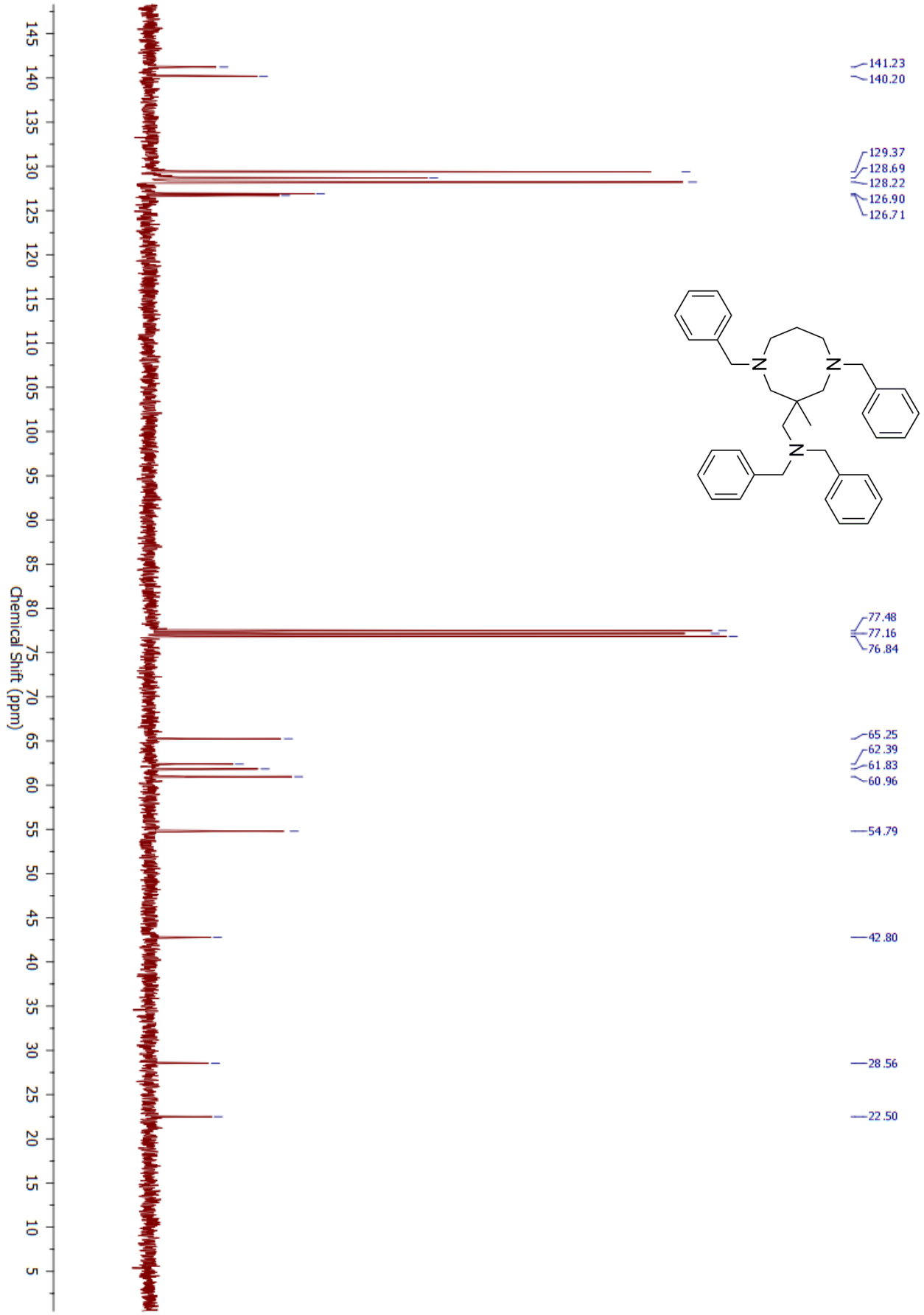

Figure S25—^{13}C NMR Spectrum of **1b**, $CDCl_3$, 100 MHz

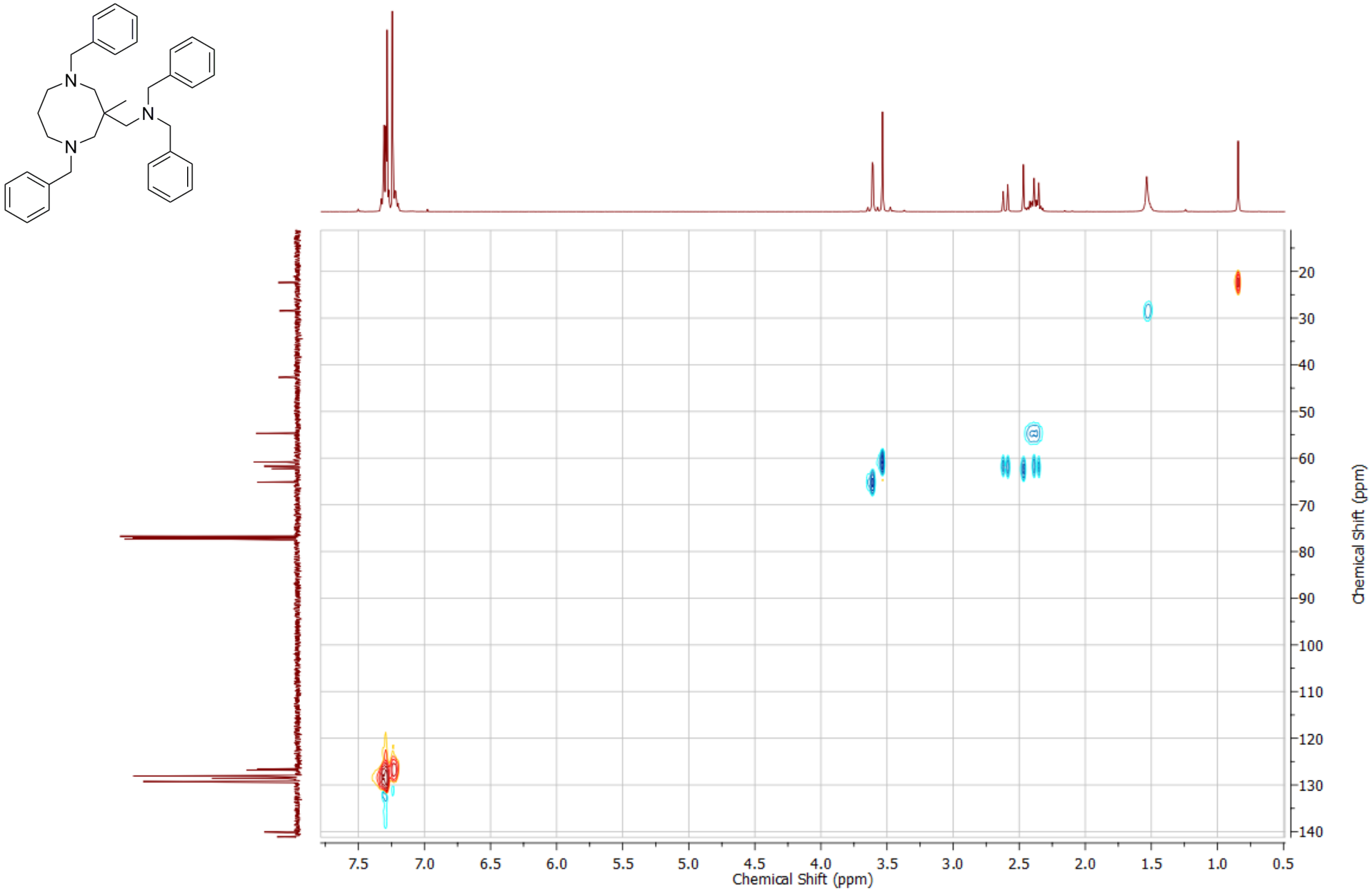

Figure S26—HSQC NMR Spectrum of **1b**, $CDCl_3$, 400 MHz.

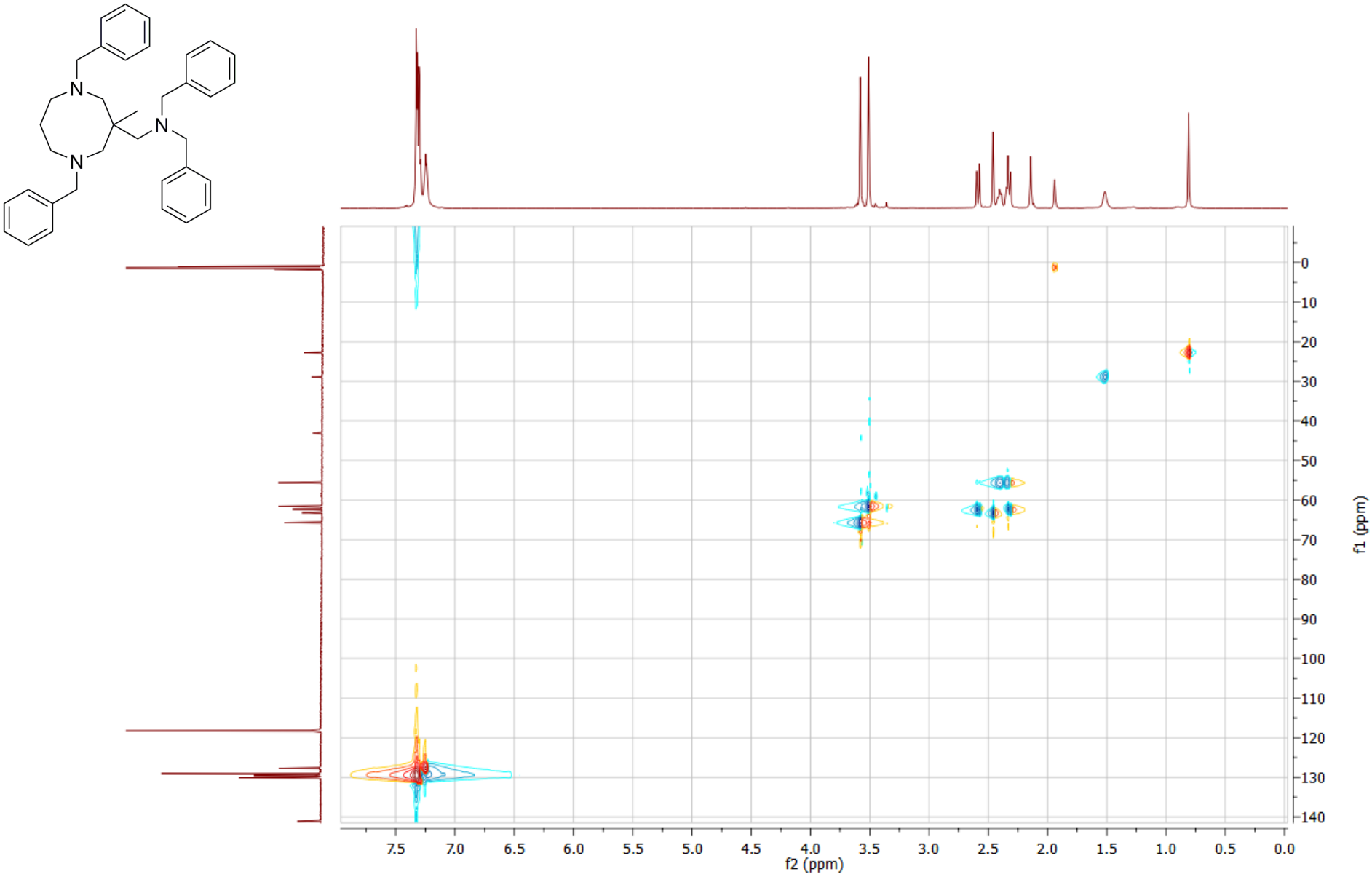

Figure S27—HSQC NMR Spectrum of **1b**, CD_3CN, 600 MHz. The HSQC of **1b** in CD_3CN is shown for comparative purposes with the NMR data provided for **[1b·H](PF_6)]** and **[1b·2H]($OTf)_2$**.

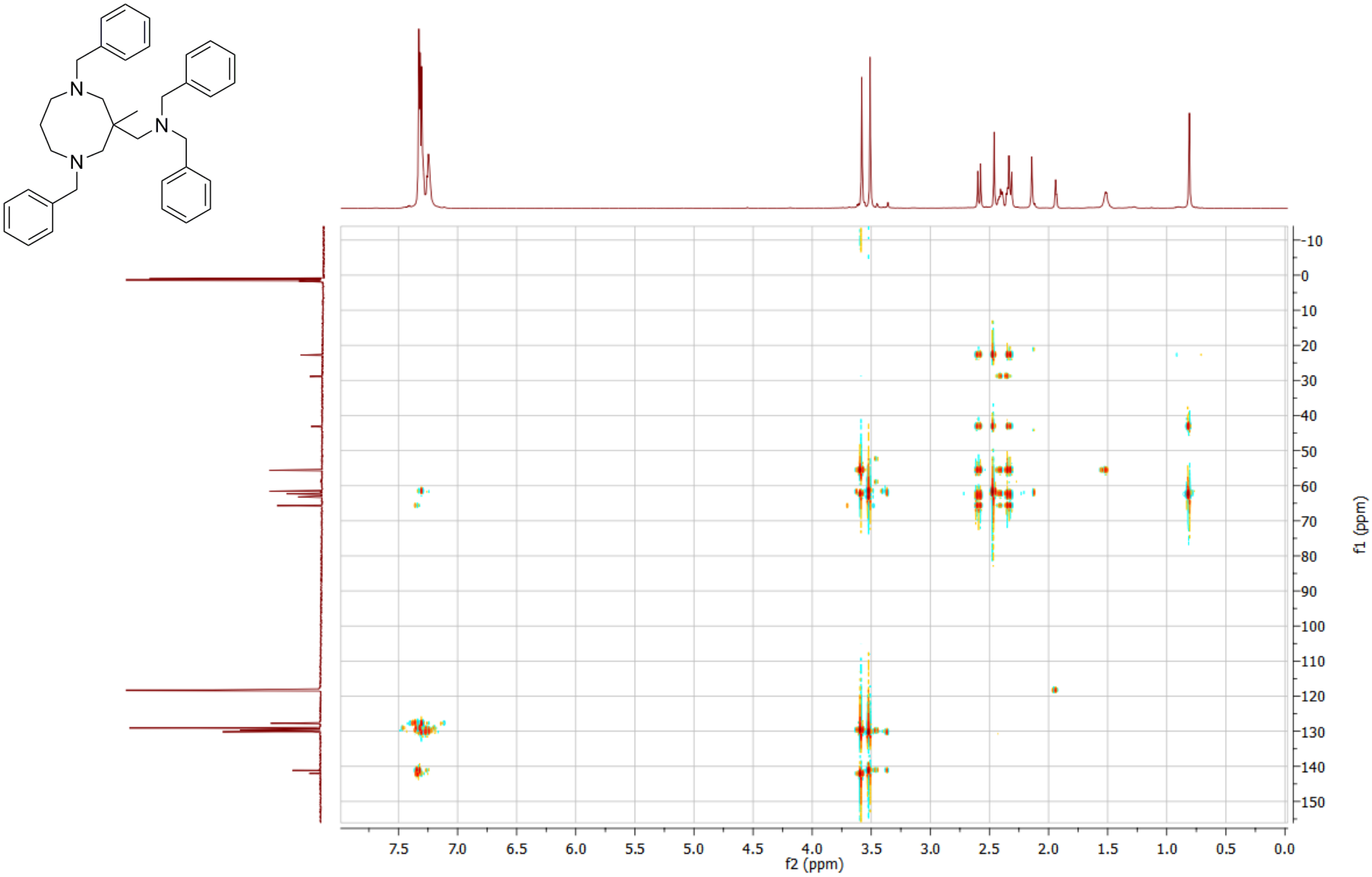

Figure S28—HMBC NMR Spectrum of **1b**, CD_3CN, 600 MHz. The HSQC of 1b in CD3CN is shown for comparative purposes with the NMR data provided for **[1b·H](PF6)]** and **[1b·2H](OTf)$_2$**.

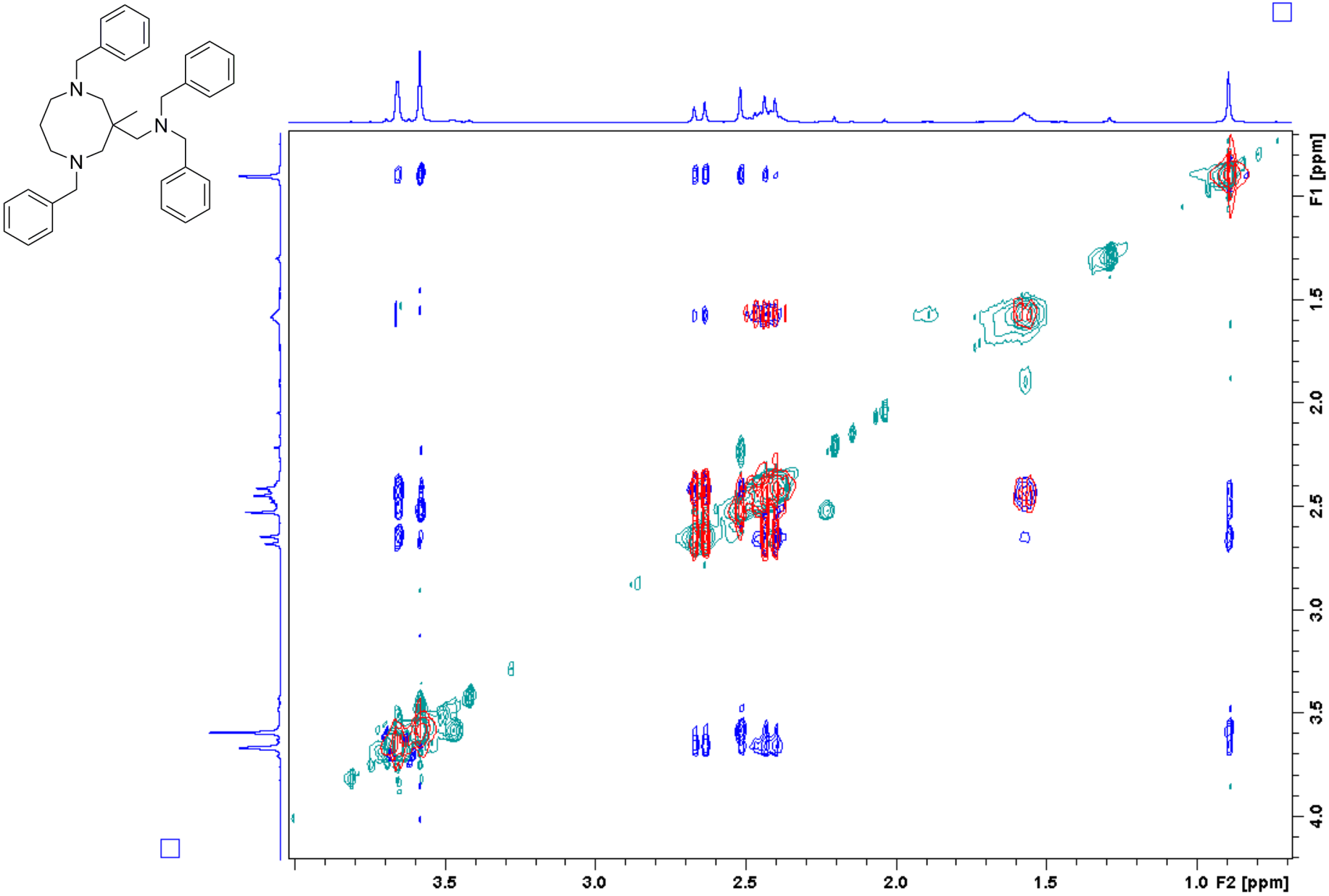

Figure S29—2d ^{1}H NOSEY NMR ($CDCl_3$, 400 MHz) Spectrum (Blue/Green) of **1b** showing through space coupling overlaid with the ^{1}H -^{1}H COSY of **1b** (Red) showing through bond coupling. Peaks appearing in both spectra are through bond and subsequently the remaining peaks are definitively through space.

Figure S30—^{1}HNMR Spectrum of **[1b·H](PF$_6$)**, $CDCl_3$, 400 MHz

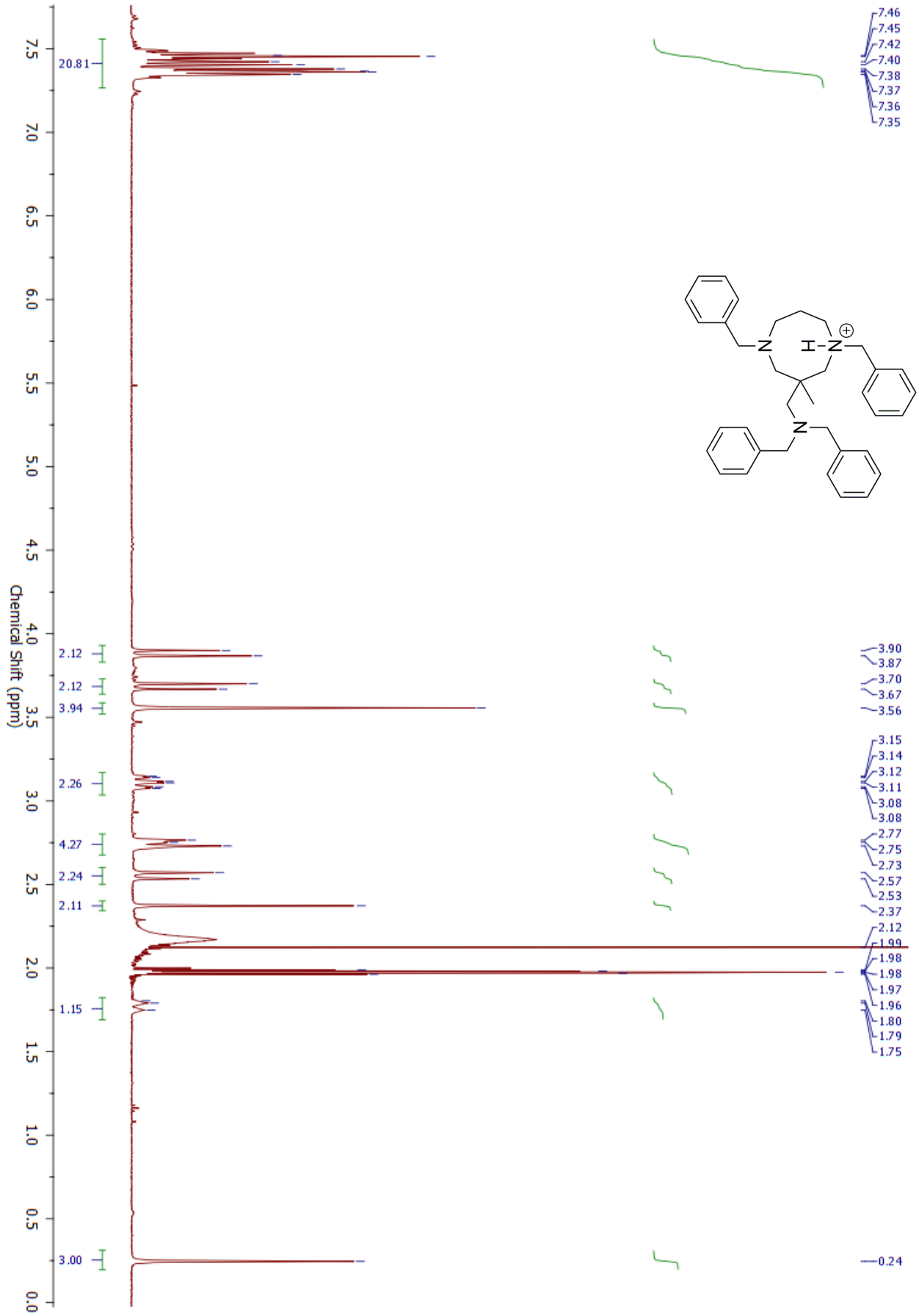

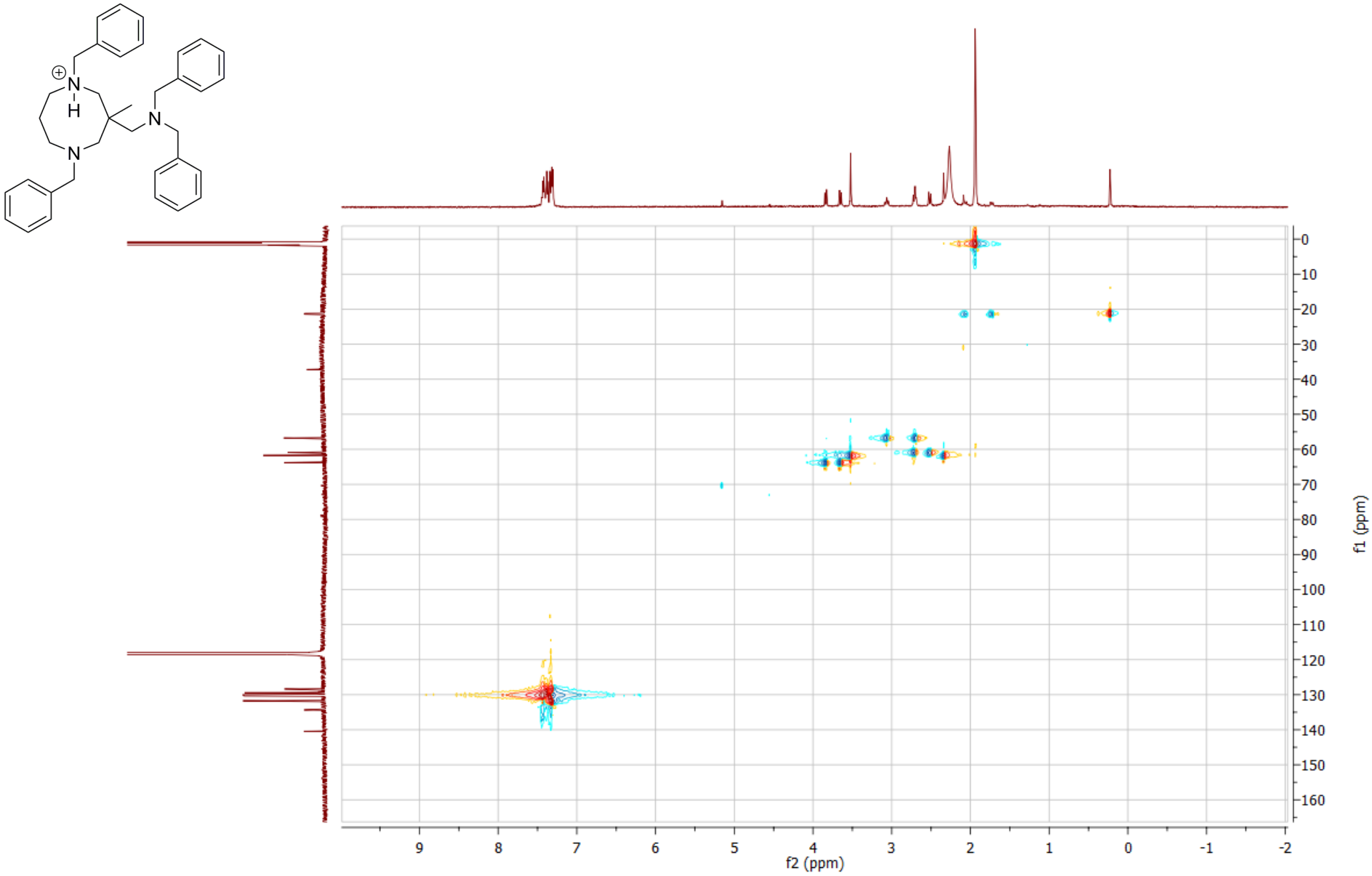

Figure S31—HSQC NMR Spectrum of **[1b·H](PF$_6$)**, CD_3CN, 600 MHz

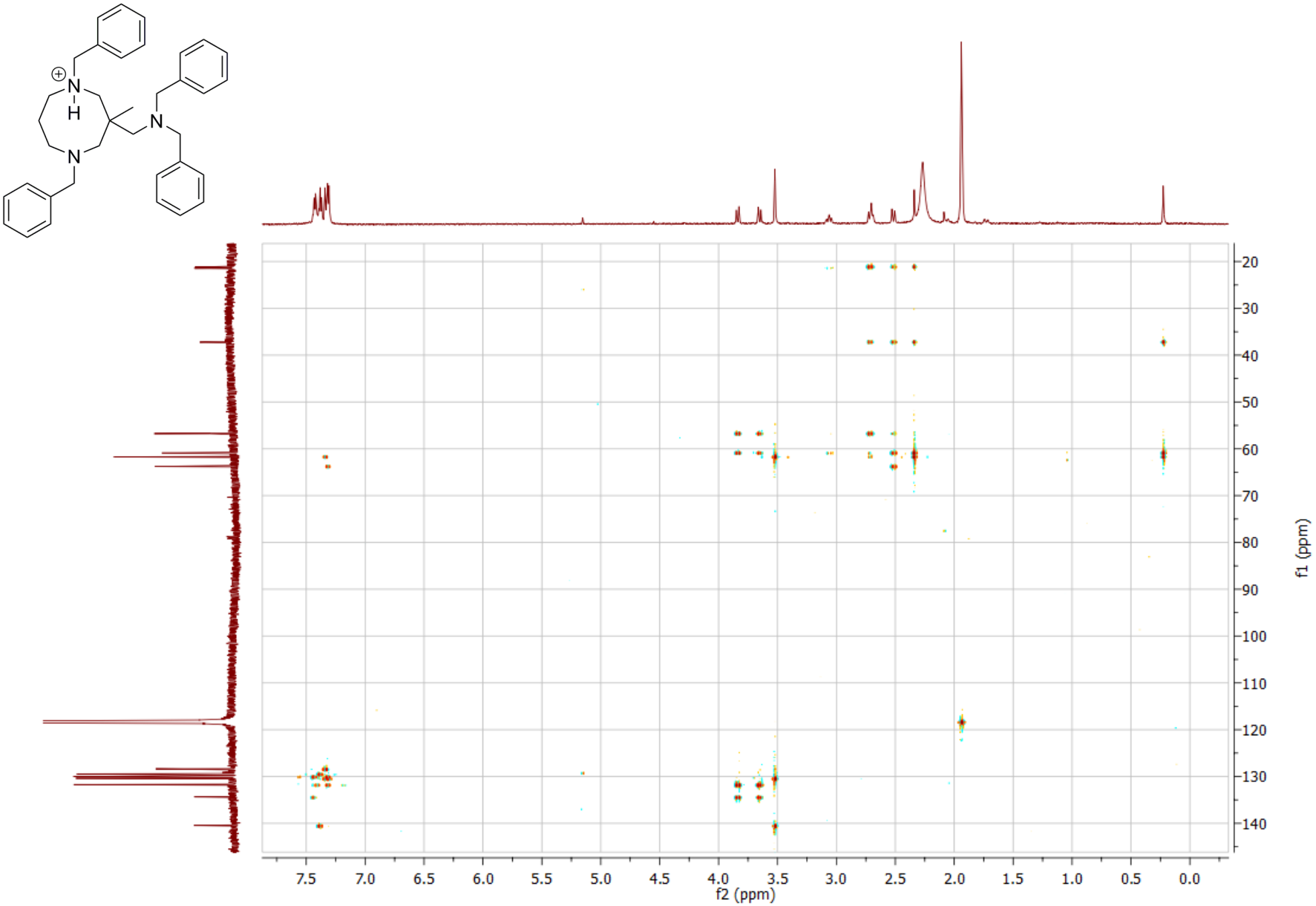

Figure S32—HMBC NMR Spectrum of **[1b·H](PF$_6$)**, CD_3CN, 600 MHz

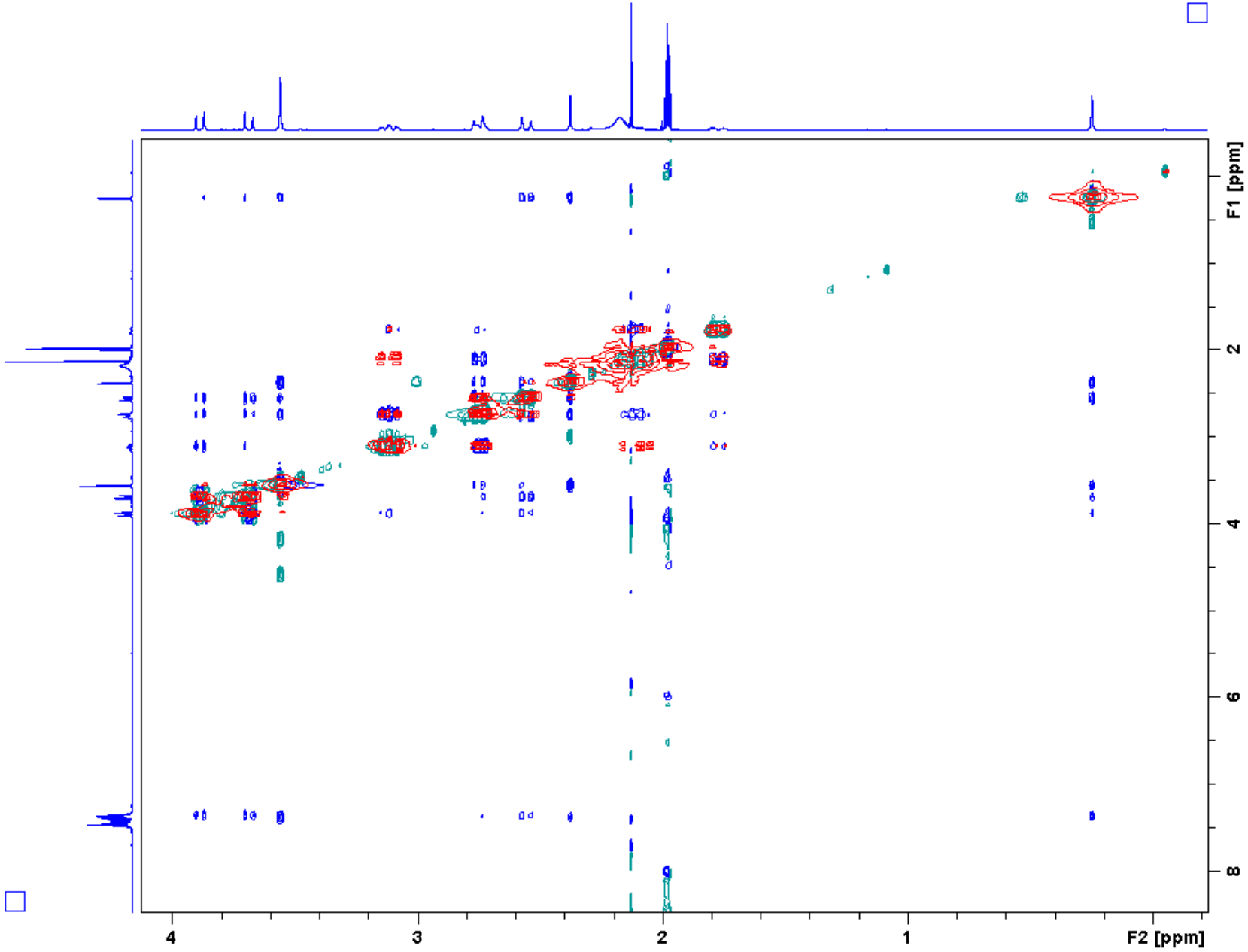

Figure S33—2d ^{1}H NOSEY NMR ($CDCl_3$, 400 MHz) Spectrum (Blue/Green) of **[1b·H](PF_6)** showing through space coupling overlaid with the ^{1}H -^{1}H COSY of **[1b·H] (PF_6)** (Red) showing through bond coupling. Peaks appearing in both spectra are through bond and subsequently the remaining peaks are definitively through space.

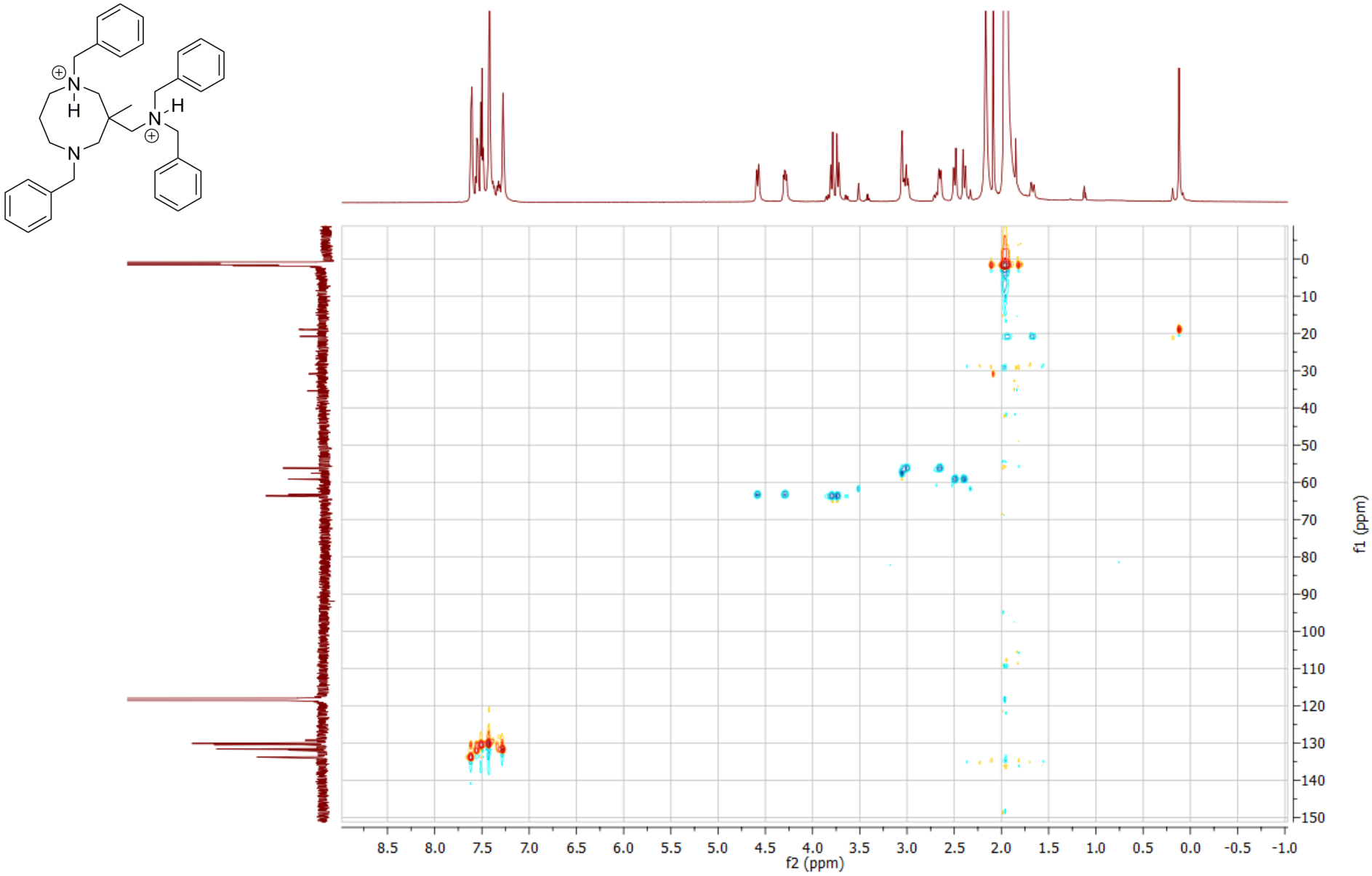

Figure S34—HSQC NMR Spectrum of **[1b·2H](OTf)$_2$**, CD_3CN, 600 MHz

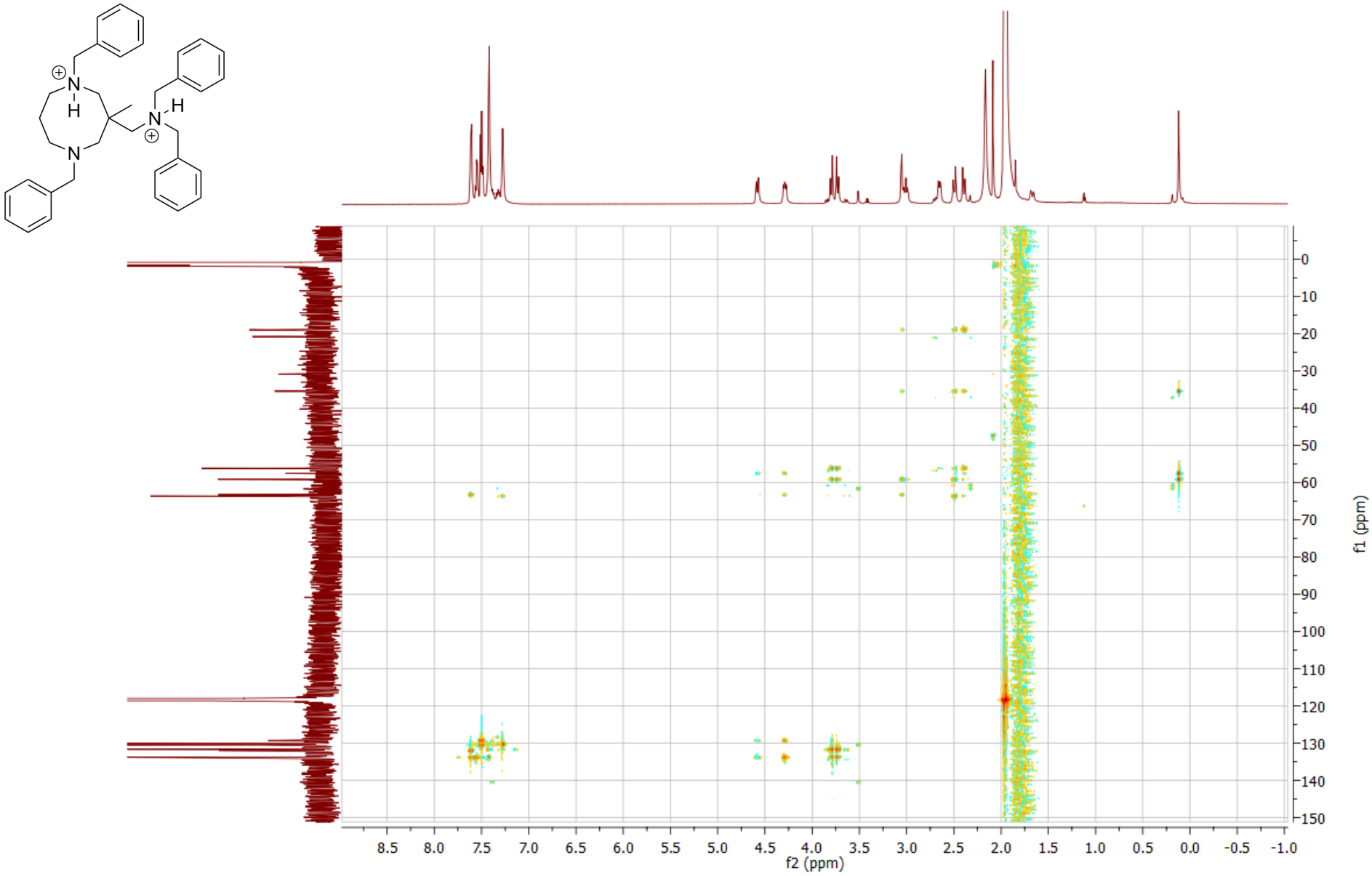

Figure S35—HMBC NMR Spectrum of **[1b·2H](OTf)$_2$**, CD_3CN, 600 MHz

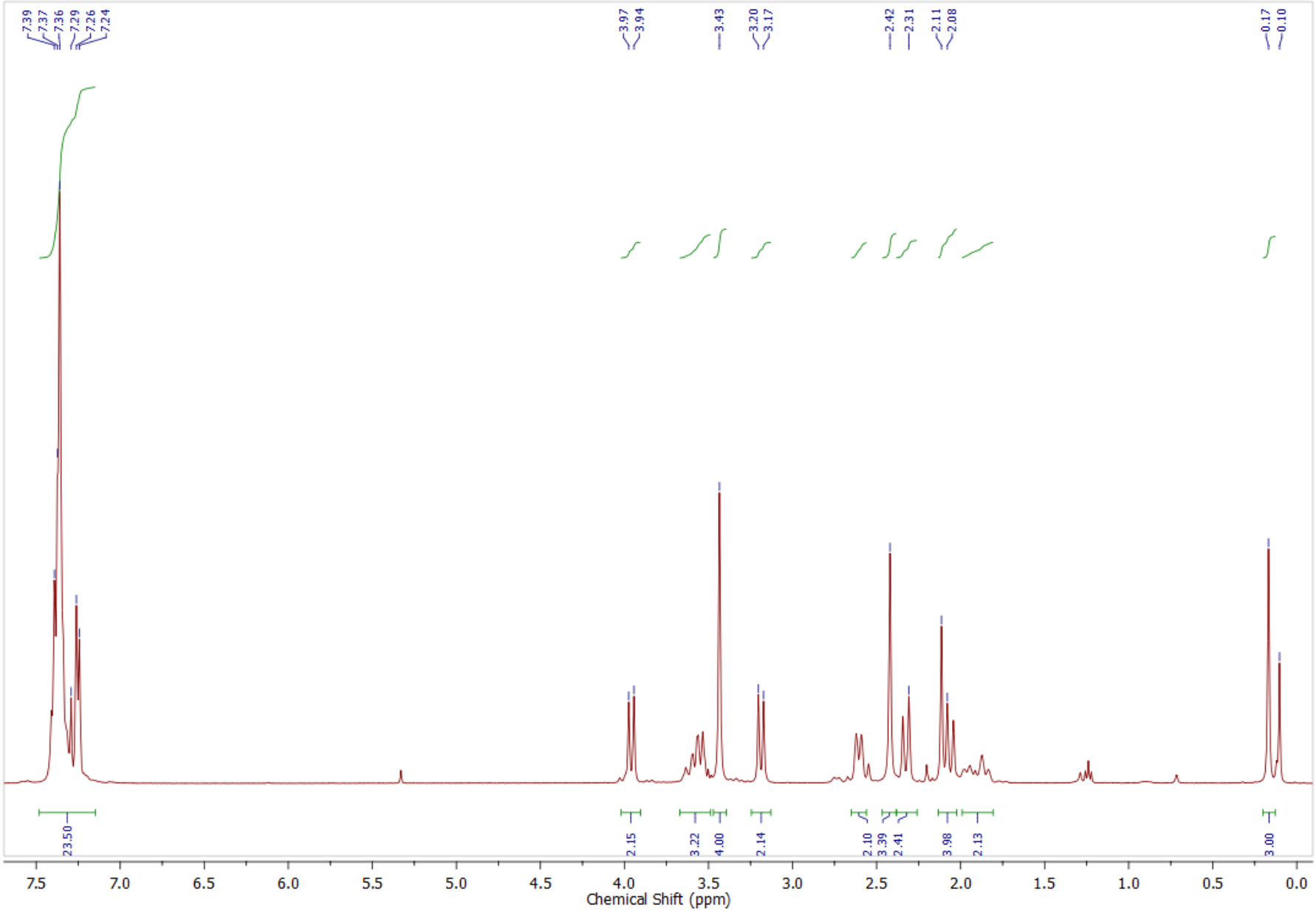

Figure S36— ^{1}H NMR Spectrum of **22** $CDCl_3$, 400 MHz

Figure S37— ^{13}C NMR Spectrum of **22** $CDCl_3$, 400 MHz

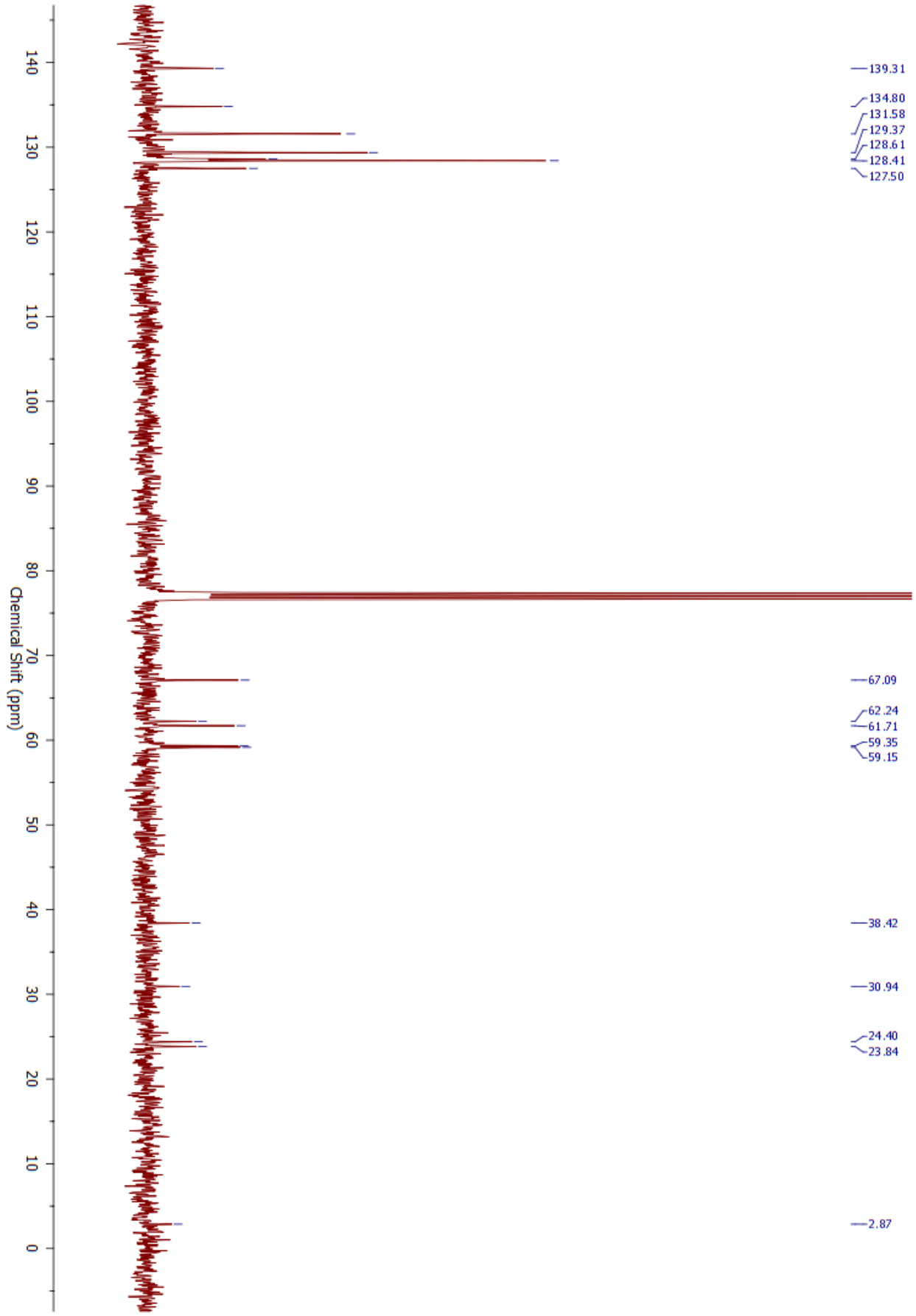

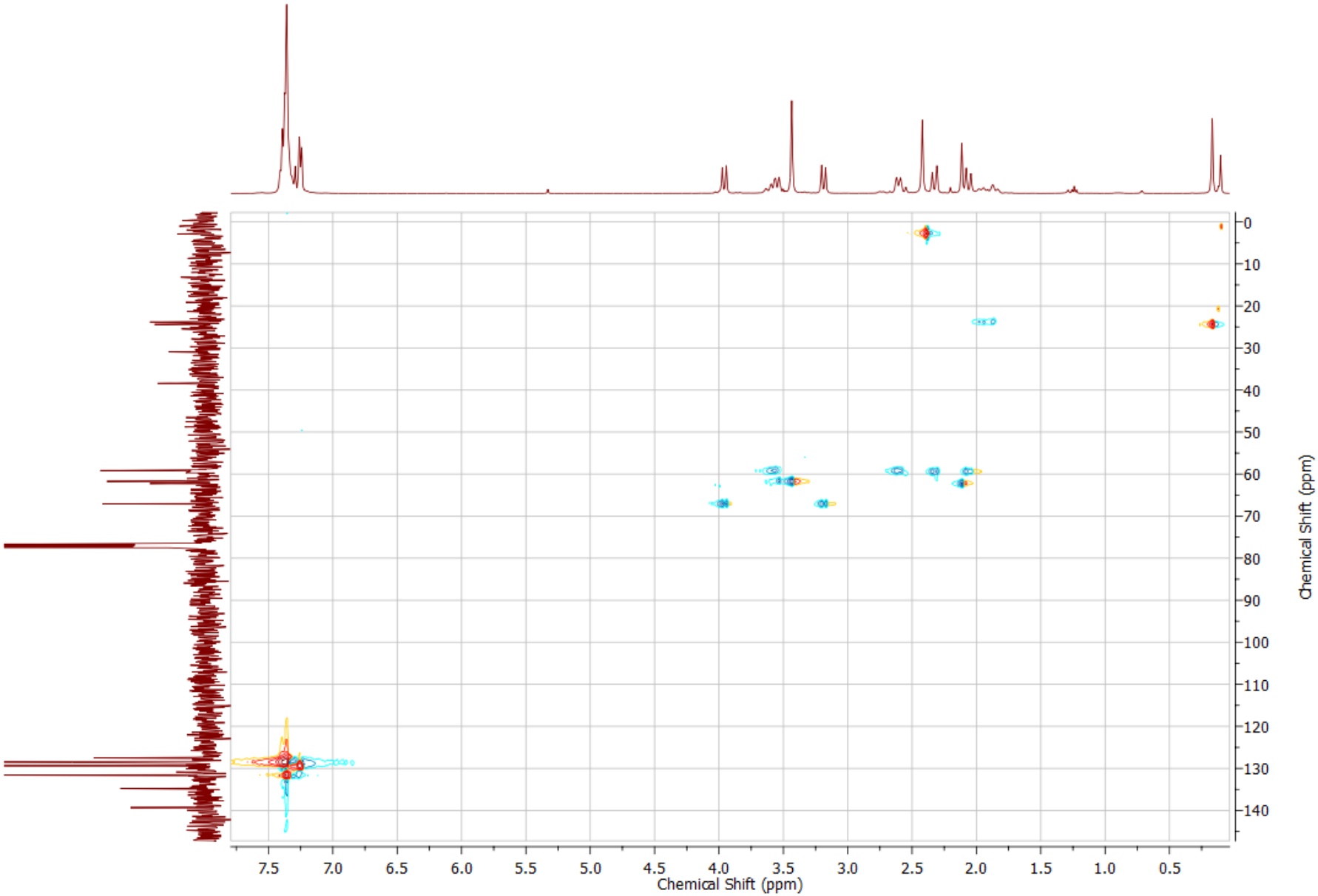

Figure S38—HSQC NMR Spectrum of **22** $CDCl_3$, 400 MHz